



# Diesel soot elimination over potassium-promoted $\text{Co}_3\text{O}_4$ nanowires monolithic catalysts under gravitation contact mode

Chunmei Cao<sup>a</sup>, Lingli Xing<sup>a</sup>, Yuexi Yang<sup>a</sup>, Ye Tian<sup>a</sup>, Tong Ding<sup>a</sup>, Jing Zhang<sup>b</sup>, Tiandou Hu<sup>b</sup>, Lirong Zheng<sup>b</sup>, Xingang Li<sup>a,\*</sup>

<sup>a</sup> Collaborative Innovation Center of Chemical Science and Engineering (Tianjin), Tianjin Key Laboratory of Applied Catalysis Science & Engineering, School of Chemical Engineering & Technology, Tianjin University, Tianjin 300072 PR China

<sup>b</sup> Beijing Synchrotron Radiation Facility, Institute of High Energy Physics, Chinese Academy of Sciences, Beijing 100049, PR China

## ARTICLE INFO

### Article history:

Received 9 March 2017

Received in revised form 7 June 2017

Accepted 12 June 2017

Available online 15 June 2017

### Keywords:

$\text{Co}_3\text{O}_4$  nanowires

Monolithic catalysts

Soot combustion

Gravitational contact mode

Potassium

## ABSTRACT

Herein, we report the high catalytic activity of the potassium-promoted  $\text{Co}_3\text{O}_4$  nanowires supported on the monolithic three-dimensional macroporous (3-DM) nickel foam substrate (xKCo-NW) for soot combustion. The 3-DM structure of Ni foam and the space among these nanowires can extremely improve the contact efficiency between soot and catalysts. Loading of potassium provides the new active sites for soot oxidation, improves catalyst-soot contact as a molten salt and increases the number of the surface adsorbed oxygen species. The 5KCo-NW catalyst loaded with 5% potassium shows the highest catalytic performance, as well as a high water resistance. There are two types of potassium species in the catalysts, most potassium species is in the form of separate phases, and few interacts with cobalt oxide. The interaction between potassium species and cobalt oxide stabilizes a part of potassium species, and the stabilized potassium species can promote the catalytic activity for the consecutive soot combustion cycle. Moreover, our results show that the chemisorbed  $\text{NO}_x$  species on the 5KCo-NW catalyst are more active than the gaseous  $\text{NO}_2$  for soot oxidation. In the presence of  $\text{O}_2$ , soot combustion is accelerated to react with the chemisorbed  $\text{NO}_x$  species; whereas the formed nitrate/nitrite species are catalytically inert.

© 2017 Elsevier B.V. All rights reserved.

## 1. Introduction

Diesel engines have been widely employed due to its high fuel efficiency, low-operating cost and high perdurability under the lean condition. However, soot particulates emitted by diesel engines cause serious health and environment problems [1–6]. Currently, the catalytic combustion technique combined with diesel particulate filters (DPFs) is regarded as an efficient after-treatment for soot clean-up through a relatively complex gas-solid-solid reaction [7,8]. For this after-treatment technology, the exploitation of the oxidation catalyst is one of the important challenges, which requires low cost and high soot oxidation performances including low soot ignition temperatures and high thermal stabilities. The Cu/ZnO and Au/ZnO catalysts synthesized by G. Corro et al. showed the lower soot ignition temperature of  $\sim 150^\circ\text{C}$  [9–11].

The catalytic soot oxidation reaction is a typical redox process in nature, which takes place at the “triple-phase contact points”

among gaseous reactants ( $\text{O}_2$  and/or  $\text{NO}_x$ ), solid soot particulates and solid catalysts. Since soot particulates have a large particulate size (25–100 nm), it is difficult to access the inner surface of micropores or mesopores in these powder catalysts. So, the design and choice of soot oxidation catalysts usually proceed in the following ways. The first way is to enhance the reducibility of the catalysts by adding additives [12], improving interaction between active components and supports [13,14], doping ions [15] and adopting composite oxides [16,17]. The second way is to promote the oxygen spillover through supporting or doping alkali metal to form highly mobilized active oxygen [18–20]. The third way is to improve the contact efficiency between soot particulates and catalysts by modulating the microstructure of the catalyst and loading the component with relatively low melting point, such as adopting nano-catalysts to increase contact area [21], preparing macroporous catalysts [22–24], and supporting potassium-containing compounds [25,26]. According to the previous reports [7,27–29], the monolithic catalysts possessing open macropores facilitate the contact between catalysts and soot particulates and extremely improved the catalytic performances for soot combustion.

\* Corresponding author.

E-mail address: [xingang.li@tju.edu.cn](mailto:xingang.li@tju.edu.cn) (X. Li).

Potassium-including compounds, for instance,  $K_2O$ ,  $KNO_3$  and  $K_2CO_3$ , can serve as the independent catalysts or the active components for soot oxidation and possess a high performance [30]. In addition, potassium is an excellent  $NO_x$  storage component, and the nitrate/nitrite originated from the storage of  $NO_x$  on potassium can act as a molten salt to improve catalyst-soot contact by increasing surface mobility [31–33]. Herein, a series of potassium-promoted  $Co_3O_4$  nanowires on three-dimensional macroporous (3-DM) nickel foam (Ni foam) substrate ( $xKCo$ -NW) was successfully synthesized through a simple hydrothermal and impregnation method, and showed excellent catalytic activities for soot combustion under gravitation contact mode (abbreviated as GCM), especially for the 5KCo-NW catalyst. The GCM was employed to achieve the loose contact condition between catalysts and soot particulates. In the whole process of mixing soot with catalyst, the deposition of soot on catalyst surface is driven by the gravity, and no grinding or mechanical mixing was performed [28,29]. In order to investigate the relationship between the physical and chemical properties of the as-prepared catalysts and the catalytic activities for soot combustion, multiple characterization experiments were carried out, such as the X-ray diffraction (XRD), the extended X-ray absorption fine structures (EXAFS), the scanning electron microscopy (SEM), the transmission electron microscopy (TEM), X-ray photoelectron spectroscopy (XPS), the temperature-programmed reduction by soot (soot-TPR) measurements and the temperature-programmed oxidation by NO (NO-TPO). Moreover, in order to investigate the existence state of the active  $NO_x$ , the temperature programmed oxidation experiments for soot (soot-TPO) were carried out under the different conditions. Based on the results of characterization and catalytic activities, the  $NO_x$ -aided soot combustion mechanism was discussed in detail.

## 2. Experimental section

### 2.1. Synthesis of the $Co_3O_4$ nanowires on nickel foam (Co-NW)

$Co_3O_4$  nanowires on the 3-DM Ni foam were prepared through a simple hydrothermal method [34]. Typically, a piece of clean Ni foam (about  $2.5\text{ cm} \times 5\text{ cm}$ , the Ni foam purchased from LIZHIYUAN battery materials Co. Ltd., the mechanical strength of Ni foam is more than 1 MPa, the thickness of Ni foam is 1.7 mm and the porosity is more than 98%) was put in Teflon-lined stainless steel autoclave with 50 mL homogeneous solution concluding 1 mmol of  $Co(NO_3)_2 \cdot 6H_2O$ , 2 mmol  $NH_4F$  and 5 mmol of  $CO(NH_2)_2$ . After 5 h growth at  $120^\circ\text{C}$ , the as-prepared precursors were calcined in air at  $500^\circ\text{C}$  for 2 h, denoted as Co-NW.

### 2.2. Preparation of the $xKCo$ -NW catalysts

The Co-NW loaded potassium catalysts with adjustable potassium content were synthesized through a facile wet impregnation method. The precursor of the Co-NW was immersed into 0.1 M, 0.5 M and 1.0 M  $CH_3COOK$  aqueous solution for 60 min, respectively. The as-prepared precursors were dried at  $120^\circ\text{C}$  for 12 h, and then annealed at  $500^\circ\text{C}$  in air for 2 h to get the final catalysts, denoted as  $xKCo$ -NW ( $x$  is on behalf of the mass fraction of potassium in the catalyst without Ni foam substrate). The mass percentages of potassium element in different samples were about 1%, 5% and 10% corresponding to the 0.1 M, 0.5 M and 1.0 M  $CH_3COOK$  solutions through inductively coupled plasma (ICP) method (Vista MPX instrument), which denoted as 1KCo-NW, 5KCo-NW and 10KCo-NW, respectively.

### 2.3. Preparation of the $Pt/Al_2O_3$ sample

The  $Pt/Al_2O_3$  sample was prepared by incipient wetness impregnation of  $\gamma$ - $Al_2O_3$  support (purchased from Aladdin with the surface area of  $150\text{ m}^2\text{ g}^{-1}$ ) with appropriate amounts of an aqueous solution of  $H_2PtCl_6 \cdot 6H_2O$ . The impregnated powders dried at  $120^\circ\text{C}$  overnight, and then annealed at  $500^\circ\text{C}$  in air for 2 h. The weight loading of Pt in the sample is 1%, which was determined by the inductively coupled plasma (ICP) method using a Vista MPX instrument.

### 2.4. Characterizations

XRD characterizations were performed on Rigaku D/Max-2500 diffractometer system using  $Cu K_{\alpha 1}$  ( $\lambda = 0.15409\text{ nm}$ ) as radiation source.

X-ray absorption spectra of Co  $K$ -edge were recorded on the XAFS station in 1W1B beamline of Beijing Synchrotron Radiation Facility.

SEM images and EDS mapping were carried out on a field emission scanning electron microscope with a Hitachi S-4800. TEM images were obtained by using a JEOL-JEM-2100F electron microscope.

XPS experiments were performed on a PHI-1600 ESCA spectrometer using  $Mg K_{\alpha}$  radiation (1253.6 eV) as radiation source. The binding energy was calibrated using C 1s peak at 284.6 eV as standard and quoted with a precision of  $\pm 0.2\text{ eV}$ .

Soot-TPR test was performed as the carbon thermal reduction without gaseous oxygen in a fixed-bed reactor. The mixture (10 mg) under gravitation contact mode was heated up to  $750^\circ\text{C}$  in  $N_2$  atmosphere. The productions of  $CO_2$  and CO were on-line analyzed by infrared gas analyzer.

NO-TPO experiments were performed on the above fixed beds. Pure catalysts (100 mg) without addition of soot were heated from 100 to  $600^\circ\text{C}$  in the 400 ppm NO, 5%  $O_2$  and  $N_2$  balanced gas at a flow rate of  $100\text{ mL min}^{-1}$  under normal conditions. The  $NO_2$  concentration in the outlet gas was online monitored by the Chemiluminescence NO- $NO_2$ - $NO_x$  Analyzer.

### 2.5. Activity evaluation

The catalytic activities were estimated by the soot-TPO using Printex-U soot purchased from Degussa as the model soot conducting in the fixed bed micro-reactor. The GCM was employed to achieve the loose contact condition between catalysts and soot particulates, in which soot was dispersed in ethanol under ultrasonic assistance (0.5 mg soot per 1 mL ethanol), and then the dispersed suspension (2 mL) was dropped on the prepared catalysts. Thereafter, the mixture (the mass ratio of catalysts and soot is 10/1) was dried at  $60^\circ\text{C}$  for 2 h [35]. Additionally, according to the previous report [28], the contact condition between the soot particulates and the powder catalysts under GCM is similar with that under loose contact mode. The  $Pt/Al_2O_3$  sample (50 mg) and soot particulates (5 mg) were mixed with a spatula for 5 min and obtained the loose contact mode. The mixture of soot and catalyst was pretreated in a flow of  $N_2$  ( $100\text{ mL min}^{-1}$ ) at  $200^\circ\text{C}$  for 30 min. After cooling down to room temperature, a gas  $N_2$  flow containing 0 or 600 ppm NO and 5%  $O_2$  ( $100\text{ mL min}^{-1}$ ) was introduced and the mixture was heated up to  $650^\circ\text{C}$  at a slope of  $2^\circ\text{C min}^{-1}$ . The productions of  $CO_2$  and CO were on-line analyzed by an infrared gas analyzer. Two parameters were derived in order to evaluate the catalytic activities: one was the temperatures at the soot conversions of 10% ( $T_{10}$ ) and 50% ( $T_{50}$ ), and the other was the  $CO_2$  selectivity ( $S_{CO_2}$ ). The soot conversion is defined as the percentage of  $CO_2$  and CO produced at each temperature and calculated according to:  $X(\%) = A_t/A_{max} \times 100\%$ , in which,  $A_{max}$  is the total peak areas of  $CO_2$  and CO,  $A_t$  is the total peak

areas of  $\text{CO}_2$  and  $\text{CO}$  at a given temperature. The  $S_{\text{CO}_2}$  was defined as  $S_{\text{CO}_2} = A_{\text{maxCO}_2} / (A_{\text{maxCO}_2} + A_{\text{maxCO}})$ , in which  $A_{\text{maxCO}}$  and  $A_{\text{maxCO}_2}$  are the total peak areas of  $\text{CO}$  and  $\text{CO}_2$ , respectively.

Soot-TPO experiments were further performed over the fresh 5KCo-NW catalyst after  $\text{NO}_x$  chemisorption. In detail, the catalyst was purged in pure  $\text{N}_2$  flow at  $350^\circ\text{C}$  for 30 min, which was then replaced by a mixture gas consisting of 400 ppm of  $\text{NO}$ , 5%  $\text{O}_2$  and balance  $\text{N}_2$  at a flow rate of  $100 \text{ mL min}^{-1}$  for  $\text{NO}_x$  chemisorption until to saturation. The catalyst was cooled down in the same atmosphere, denoted as 5KCo-NW-S. Thereafter, the soot-TPO experiments were carried out over the 5KCo-NW-S catalyst in  $\text{O}_2/\text{N}_2$  or  $\text{N}_2$  atmosphere, respectively. In addition, the mixture of soot and the 5KCo-NW-S was heated from 50 to  $190^\circ\text{C}$  and retained for 30 min to purge the  $\text{NO}_x$  species, and then heated from 190 to  $650^\circ\text{C}$  in 5%  $\text{O}_2/\text{N}_2$  ( $100 \text{ mL min}^{-1}$ ). To analyze the  $\text{NO}_x$  desorption species, the temperature-programmed desorption of  $\text{NO}_x$  ( $\text{NO}_x$ -TPD) was performed. The 5KCo-NW-S was heated from 50 to  $600^\circ\text{C}$  in the  $\text{O}_2/\text{N}_2$  atmosphere. The outlet gas of  $\text{NO}_x$  was monitored online.

To inspect the catalytic stability of the Co-NW and 5KCo-NW catalysts, five consecutive cycles of soot-TPO experiment were carried out in the flow  $\text{N}_2$  atmosphere containing 600 ppm  $\text{NO}$  and 5%  $\text{O}_2$  ( $100 \text{ mL min}^{-1}$ ). Moreover, in order to investigate the effect of water vapor, 5% water vapor was added to the feeding gas by passing through water in a glass bottle at  $35^\circ\text{C}$ . Meanwhile, other experimental conditions were the same with the tests without addition of water vapor by adjusting the flow rate of  $\text{N}_2$  carrier. The outlet gas was analyzed by an on-line infrared gas analyzer.

## 2.6. Isothermal kinetic measurement

The reaction rates for soot combustion over the as-prepare catalysts were acquired through the isothermal reactions at  $360^\circ\text{C}$  in an approximate kinetic regime, in which the conversion of soot was less than 10% (Fig. S1). The isothermal soot combustion experiments were carried out with a soot-catalyst mixture under GCM in the 5%  $\text{O}_2$  and  $\text{N}_2$  atmosphere. In order to eliminate the effect of external mass transport, the relatively large flow rate ( $150 \text{ mL min}^{-1}$ ) was used. When the  $\text{CO}_2$  concentration attained a steady state during the process of isothermal soot combustion,  $\text{O}_2$  was immediately cut off from the reactant flow and is substituted with a flow of  $\text{N}_2$ . The outlet gas from the steady state was on-line monitored using an infrared gas analyzer. The amount of active oxygen species for oxidizing soot particulates under these reaction conditions is two times than that of  $\text{CO}_2$ , which can be quantified by integrating the shaded area in Fig. S2 [36]:

$$\text{O} * \text{amount}(\text{mol g}^{-1}) = 2P_0VA \times 10^{-6} / RTm$$

$$\text{O} * \text{density}(\text{nm}^{-2}) = \text{O} * \text{amount} \times 6.02 \times 10^{23} / (S \times 10^{18})$$

Where  $P_0$  is the atmospheric pressure (Pa),  $V$  is the volumetric flow rate of gases through the reactor ( $\text{m}^3 \text{ s}^{-1}$ ),  $A$  is the integrated area of  $\text{CO}_2$  concentration as a function of time (s),  $m$  is the mass of the catalyst (g),  $R$  is the ideal gas constant,  $T$  is the room temperature (K), and  $S$  is the BET specific surface area of the catalyst ( $\text{m}^2 \text{ g}^{-1}$ ).

## 3. Results and discussion

### 3.1. Catalyst characterization

#### 3.1.1. XRD and EXAFS results

Fig. 1 displays the XRD patterns of the as-prepared samples. For the reference sample Ni foam, main diffraction peaks at  $2\theta = 44.3^\circ$ ,  $51.6^\circ$  and  $76.1^\circ$  are identified and they are attributed to (111), (200) and (220) lattice planes of metallic Ni (JPCDS 65-0380), respec-

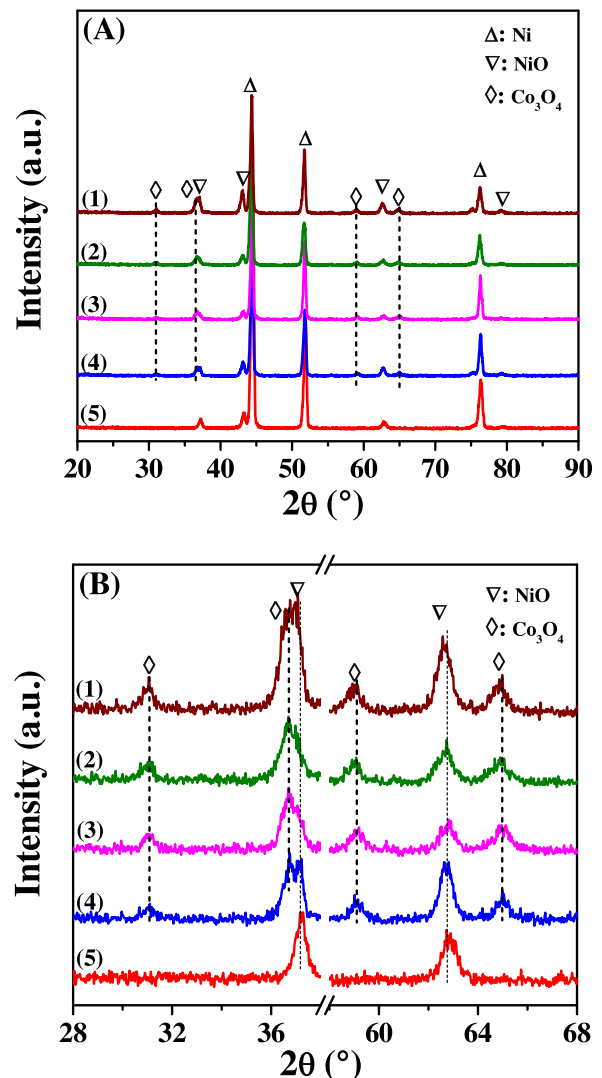
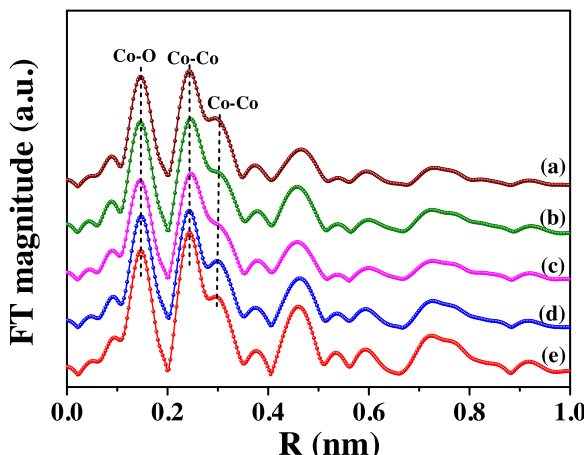


Fig. 1. XRD patterns of (1) 10KCo-NW, (2) 5KCo-NW, (3) 1KCo-NW, (4) Co-NW and (5) Ni foam: (A) full patterns; and (B) Zoom-in of (A).

tively. Moreover, minor  $\text{NiO}$  phase (JPCDS 65-2901) is also observed with the diffraction peaks at  $2\theta = 37.1^\circ, 43.1^\circ, 62.5^\circ$  and  $79.0^\circ$ . While for the Co-NW and xKCo-NW catalysts, there are four weak peaks associated with  $\text{Co}_3\text{O}_4$  appearing at  $2\theta = 31.2^\circ, 36.8^\circ, 59.3^\circ$  and  $65.2^\circ$ , which correspond to (220), (311), (511) and (400) lattice planes (JPCDS 43-1003), respectively. Fig. 1B displays the enlarged diffraction peaks of  $\text{Co}_3\text{O}_4$ . The presence of  $\text{Co}_3\text{O}_4$  in the catalysts was also verified by EXAFS results. Fig. 2 displays the radial structure functions (RSFs) of Co K-edge for the as-prepared catalysts and the reference  $\text{Co}_3\text{O}_4$ . Obviously, the RSFs of the catalysts are similar to that of the reference  $\text{Co}_3\text{O}_4$ , with similar coordination peaks around 0.155 nm, 0.254 nm and 0.303 nm, which are in agreement with the Co-O shell, the Co-Co shell and the remote Co-Co shell, respectively [24]. Thus, it can demonstrate that the cobalt in the catalyst exists as the form of  $\text{Co}_3\text{O}_4$  phase in conformity with the XRD results. However, for the potassium-containing catalysts, no diffraction peak related to potassium species appears, probably due to the low content of potassium species and their high dispersion on the surface of the  $\text{Co}_3\text{O}_4$  nanowires.

#### 3.1.2. Electron microscope characterization

Fig. 3 shows the images of SEM, TEM/HRTEM and the size distribution of the average diameter of the as-prepared catalysts, and



**Fig. 2.** Co K-edge RSFs of (a) 10KCo-NW, (b) 5KCo-NW, (c) 1KCo-NW, (d) Co-NW and (e)  $\text{Co}_3\text{O}_4$  standard.

Fig. S3 displays the images of SEM and TEM/HRTEM of the Ni foam. In Fig. S3a, the Ni foam possesses interconnected macroporous structure with the various diameters ranging from 0.2 to 0.6 mm, and its surface exhibits uneven wrinkles of  $\text{NiO}$ , in Fig. S3b. In Fig. 3a1–a4, the Co-NW catalyst exhibits the nanowire structure with an average diameter of  $\sim 64$  nm according to statistic of two hundred of nanowires from the SEM images. The nanowires are well-distributed on the skeleton frame of the Ni foam substrate (inset image in Fig. 3a1). The surface area of the Co-NW catalyst is  $115 \text{ m}^2 \text{ g}^{-1}$ , as listed in Table S1. Through the calculation from the

HRTEM image, the lattice plane spacing is 0.246 nm, which corresponds to the (311) plane of  $\text{Co}_3\text{O}_4$ . The open macropores consisted by the space among these nanowires would facilitate soot particulates deposition [37].

After supporting potassium species, the nanowire structure of the catalysts is well retained, except that the surface of the nanowire becomes rough. For the 1KCo-NW catalyst with 1% of potassium loading, the average diameter of nanowires increases from 64 to 82 nm. Probably, it is because that the  $\text{K}_2\text{CO}_3$  nanoparticles cover the surface of  $\text{Co}_3\text{O}_4$  nanowires. The surface area of the 1KCo-NW slightly reduces to  $98 \text{ m}^2 \text{ g}^{-1}$ . In addition, in the HRTEM image as displayed in Fig. 3b4, there is an amorphous material, which is identified to be  $\text{K}_2\text{CO}_3$  according to the reference [38]. With the elevation of potassium content to 5%, more potassium species nanoparticles are observed around the surface of the nanowires (Fig. 3c1) and uniformly distribute on the  $\text{Co}_3\text{O}_4$  nanowires as proved by the EDS mapping in Fig. 4. The average diameter of the nanowires has little change and retains around 81 nm, but the surface of the nanowire becomes rougher. When the amount of the supported potassium species increases to 10%, the  $\text{K}_2\text{CO}_3$  nanoparticles aggregate and totally cover on the  $\text{Co}_3\text{O}_4$  nanowires as displayed in Fig. 3d3. The average diameter of the nanowire increases from  $\sim 81$  nm to  $\sim 85$  nm, and the surface area of the 10KCo-NW reduce from 89 to  $70 \text{ m}^2 \text{ g}^{-1}$ . In addition, the aggregated  $\text{K}_2\text{CO}_3$  nanoparticles block the open macropores and decrease the contact chance between soot particulates and catalysts (inset image in Fig. 3d1). In the HRTEM images of the xKCo-NW catalysts, the amorphous  $\text{K}_2\text{CO}_3$  can be identified, which proves the existence of potassium species. The characterization results combined with XRD, EXAFS, SEM, TEM and HRTEM demonstrate that

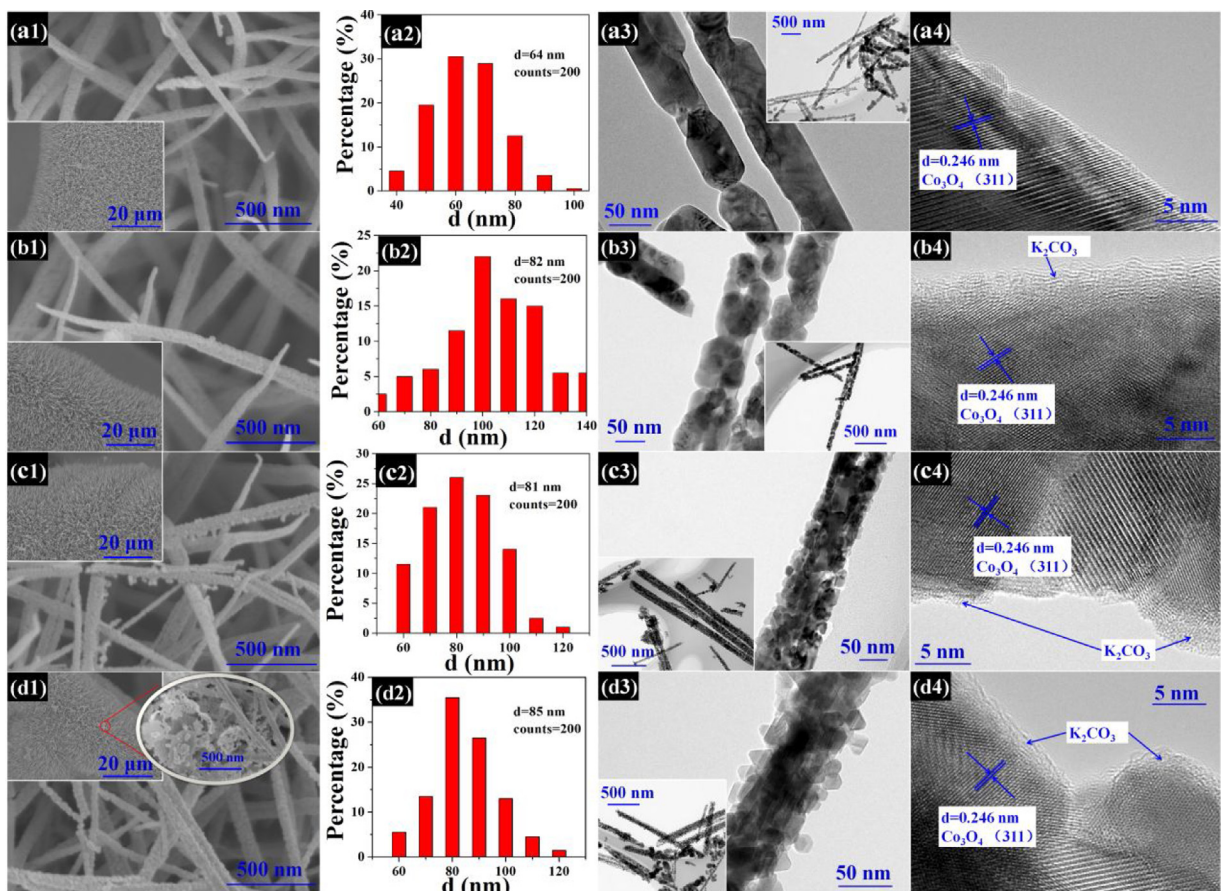


**Fig. 3.** Electron microscope characterization on the catalysts Co-NW (a1-a4), 1KCo-NW (b1-b4), 5KCo-NW (c1-c4) and 10KCo-NW (d1-d4): (a1-d1) SEM images, (a2-d2) the size distribution determined by SEM images, (a3-d3) TEM images and (a4-d4) HRTEM images.

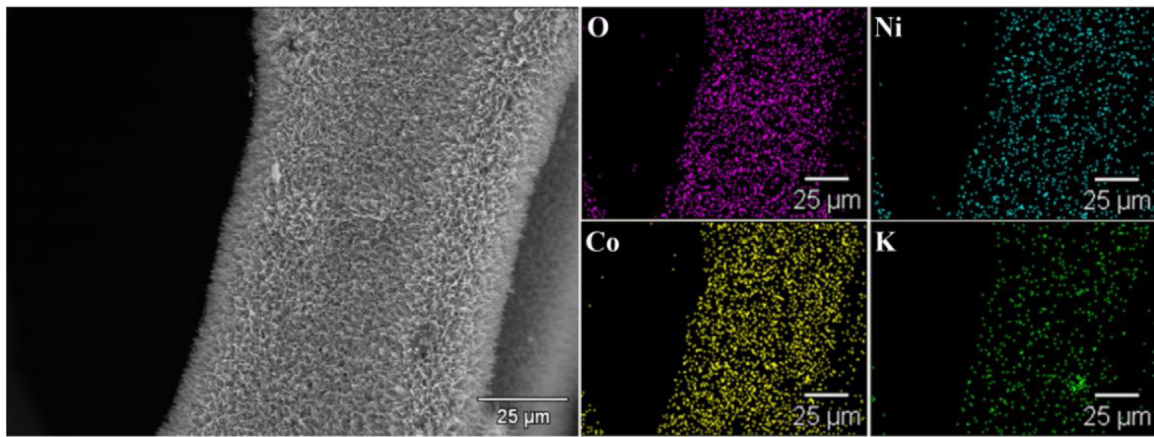


Fig. 4. EDS mapping images of the 5KCo-NW catalyst.

**Table 1**

The BE of Co 2p<sub>3/2</sub> and O 1s core levels, the ratio of O<sub>ads</sub>/O<sub>lat</sub> and the K/Co atomic ratios for the as-prepared catalysts.

Catalysts	Co 2p <sub>3/2</sub> (eV)	O 1s			K/Co
		O <sub>ads</sub> (eV)	O <sub>lat</sub> (eV)	O <sub>ads</sub> /O <sub>lat</sub>	
Co-NW	779.9	531.1/532.8	529.3	0.76	–
1KCo-NW	779.7	530.9/532.5	529.2	0.82	0.010
5KCo-NW	779.5	530.6/532.3	528.9	0.93	0.103
10KCo-NW	779.4	530.5/532.0	528.8	0.91	0.115

the as-prepared xKCo-NW samples on the 3-DM Ni foam have been successfully prepared.

### 3.1.3. XPS results

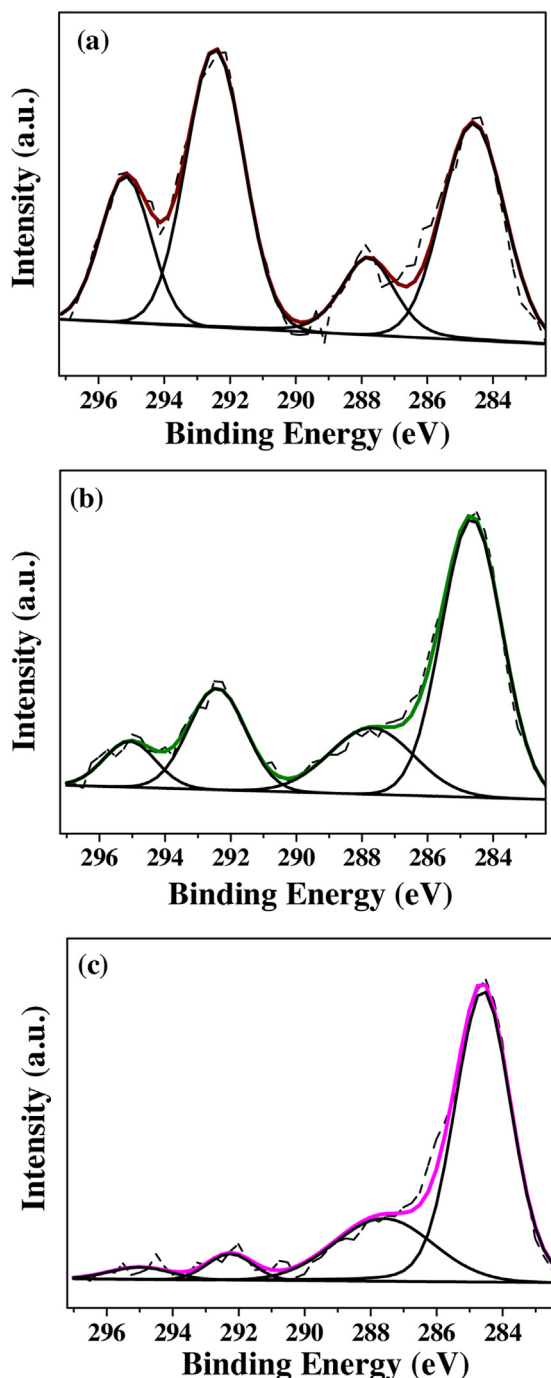
Fig. 5 displays the C 1s and K 2p XPS spectra of the as-prepared catalysts. The C 1s and K 2p spectra locate in the range of 283–290 eV and 290–297 eV, respectively. In Fig. 5, the C 1s spectra consist of two peaks corresponding with two kinds of carbon species. The C 1s peak locating at the lower binding energy (284.6 eV) is assigned as reference [39]. The higher binding energy peak at 287.9 eV can be attributed to carbonate species [25]. The doublet peaks at ~292.4 (K 2p<sub>3/2</sub>) and ~295 eV (K 2p<sub>1/2</sub>) in K 2p spectra are assigned to K<sub>2</sub>CO<sub>3</sub> [25]. So, the potassium species exist as the K<sub>2</sub>CO<sub>3</sub> phase in the catalysts.

Fig. 6 and Table 1 provide the Co 2p XPS results of the catalysts. The XPS spectra of Co 2p show typical peaks due to two spin orbit components of Co (Co 2p<sub>1/2</sub> at 795.1 eV and Co 2p<sub>3/2</sub> at 779.7 eV) and two weak satellites at the relatively higher energies (800–805 and 786–790 eV). The difference of binding energy (BE) between Co 2p<sub>1/2</sub> and Co 2p<sub>3/2</sub> peaks is 15.4 eV, and it is in accordance with the previous report for Co<sub>3</sub>O<sub>4</sub> [40,41]. The Co 2p<sub>3/2</sub> peak of the catalysts shifts to the lower binding energies with the increase of potassium loading, which demonstrates that there is interaction between K and Co due to the electron-donor effect of potassium. It would generate oxygen vacancies, as well, and the detailed discussion will be elucidated in the next part of the XPS O 1s results [42]. In addition, the surface K/Co ratio increases with the increase of potassium loading. When the potassium loading increased from 1% to 5%, the atomic ratio of K/Co increases obviously, which indicates that more Co<sub>3</sub>O<sub>4</sub> interacts with K. When the amount of the supported potassium species increases to 10%, potassium species seriously aggregated by forming the larger K<sub>2</sub>CO<sub>3</sub> particles as displayed in the inset image in Fig. 3d1. The accumulation of the K<sub>2</sub>CO<sub>3</sub> nanoparticles on the 10KCo-NW catalyst leads to exposing more Co<sub>3</sub>O<sub>4</sub> than that on the 5KCo-NW catalyst, and thus the increase of the K/Co ratio is unobvious.

Fig. 7 shows the O 1s XPS spectra of the Co-NW and xKCo-NW samples. The XPS spectra of O 1s can be deconvoluted into three peaks, the lower binding energy peak locating at ~529.0 eV corresponds to lattice oxygen (O<sub>lat</sub>) contained in metal oxides and the other two peaks locating at ~530.6 and ~532.3 eV are in accordance to the adsorbed oxygen species (O<sub>ads</sub>). Table 1 presents the results of this deconvolution, as well as the O atom ratio, the O 1s position and the ratio of O<sub>ads</sub> to O<sub>lat</sub> (O<sub>ads</sub>/O<sub>lat</sub>). Clearly, the O 1s peaks shift to lower binding energy values with the increase of potassium loading due to the electron-donor effect of potassium, and the ratio of O<sub>ads</sub>/O<sub>lat</sub> increase and then decrease slightly with the increase of potassium loading. In general, the surface adsorbed oxygen species are generated through the adsorption of gaseous O<sub>2</sub> on the oxygen vacancies existing in catalysts [43]. So, the potassium-including catalysts possess more surface adsorbed oxygen species than the catalyst without potassium. On the one hand, K<sub>2</sub>CO<sub>3</sub> can adsorb the gaseous O<sub>2</sub> and increase the amount of the adsorbed oxygen; on the other hand, the interaction between potassium and Co<sub>3</sub>O<sub>4</sub> can lead to the formation of oxygen vacancies and increase the amount of the adsorbed oxygen species. In Table 1, the relative ratio of O<sub>ads</sub> to O<sub>lat</sub> for the as-prepared catalysts can be arranged in the following order: 5KCo-NW > 10KCo-NW > 1KCo-NW > Co-NW. Obviously, the 5KCo-NW possesses the largest amount of surface adsorbed oxygen species as well as the largest amount of oxygen vacancies. Notably, although the 10KCo-NW catalyst contains the higher amount of potassium, it possesses the less amounts of the surface adsorbed oxygen species, as compared with the 5KCo-NW catalyst. Probably, the aggregation of the K<sub>2</sub>CO<sub>3</sub> nanoparticles as observed in Fig. 3d3, induces a poor contact with the Co<sub>3</sub>O<sub>4</sub> nanowires when the content of the supported potassium increased to 10%.

### 3.1.4. Soot-TPR

Fig. 8 shows the soot-TPR of the as-prepared catalysts. In the process of soot-TPR, the soot particulates in contact with the catalysts can only be oxidized by the surface oxygen species existing on the catalysts because of the absence of gaseous oxygen. In Fig. S4, no CO<sub>2</sub> signal was observed in the profile of CO<sub>2</sub>-TPD, indicating that few carbonates and/or chemisorbed CO<sub>2</sub> exists on the catalyst. Moreover, the CO concentration monitored online is 0 ppm. According to the CO<sub>2</sub> peak position, the profiles can be partitioned into three temperature regions, which are in accordance with the surface adsorbed oxygen (350–500 °C), sub-surface oxygen (450–650 °C), and bulk oxygen (>650 °C) denoted as  $\alpha$ ,  $\beta$ , and  $\gamma$ , respectively [8,42]. According to the temperature zone (320–520 °C) for soot combustion over these catalysts, soot particulates should be mainly oxidized by the surface adsorbed oxygen and sub-surface oxygen species, which are thought as the main



**Fig. 5.** XPS spectra of C 1s and K 2p of (a) 10KCo-NW, (b) 5KCo-NW and (c) 1KCo-NW. The dash line is the experimental data, and the solid line is the peak fitting data.

active oxygen species. In Fig. 8, comparing with the catalyst without potassium,  $\alpha$  and  $\beta$  peaks shift to the lower temperatures. It indicates that the interaction between potassium and  $\text{Co}_3\text{O}_4$  enhances the oxidation ability of the xKCo-NW catalysts and promotes the mobility of lattice oxygen. The results of soot-TPR over the as-prepared catalysts are in good accordance with the results of XPS. Additionally, considering the low melting points of the potassium-related phase in the potassium-containing catalysts, an additional promotion in soot oxidation could not be neglected due to the enhanced contact chance between soot and catalysts or the enhanced formation of carbonate intermediates [31].

**Table 2**

$T_{10}$  and  $T_{50}$ , and the  $\text{CO}_2$  selectivity ( $S_{\text{CO}_2}$ ) during soot combustion in the presence or absence of 600 ppm NO over the different catalysts.

Catalysts	$T_{10}$ (°C)		$T_{50}$ (°C)		$S_{\text{CO}_2}$ (%)	
	0 ppm	600 ppm	0 ppm	600 ppm	0 ppm	600 ppm
Blank	–	526	–	584	–	50.8
Ni foam	471	439	518	527	100	100
Co-NW	397	329	466	387	100	100
1KCo-NW	386	288	450	341	100	100
5KCo-NW	372	279	408	324	100	100
10KCo-NW	378	283	419	327	100	100
Pt/ $\text{Al}_2\text{O}_3$	–	321	–	384	–	100

### 3.2. Catalytic soot combustion

#### 3.2.1. Catalytic soot combustion activities

Fig. 9A displays the catalytic performance for diesel soot oxidation evaluated by TPO method in the  $\text{O}_2$  atmosphere balanced by  $\text{N}_2$  under GCM. In Fig. 9A, soot combustion without catalyst (blank) takes place at rather high temperatures. The ignition temperature of  $T_{10}$  decreases from 526 to 471 °C for soot combustion over the 3-DM Ni foam. After the  $\text{Co}_3\text{O}_4$  nanowires grow on the 3-DM Ni foam, the catalytic activity for soot combustion is improved obviously, reflecting the high redox property of the  $\text{Co}_3\text{O}_4$  nanowires. Moreover, after loading of potassium, the as-prepared catalysts further enhance the catalytic performance, showing the lower  $T_{10}$  and  $T_{50}$  temperatures. Especially, the 5KCo-NW shows the lowest  $T_{10}$  (372 °C) and  $T_{50}$  (408 °C).

In the  $\text{NO}_x$ -aided catalytic soot combustion process,  $\text{NO}_2$  is a much more active than  $\text{O}_2$  [44]. In order to demonstrate the role of  $\text{NO}_x$  in the soot combustion process, we also tested the catalytic activity of the as-prepared catalysts in the 600 ppm NO and 5%  $\text{O}_2$  atmosphere. Fig. 9B shows the catalytic performance for soot combustion under this condition. After introducing of 600 ppm NO to the flow of 5%  $\text{O}_2$  and  $\text{N}_2$ , much higher catalytic performance for soot combustion is achieved, showing lower  $T_{10}$  and  $T_{50}$  than those in the  $\text{O}_2$  atmosphere as listed in Table 2. However, most of  $\text{NO}_x$  is NO in diesel exhaust, and thus, the ability for NO oxidation to  $\text{NO}_2$  is a key factor influencing the catalytic soot combustion [45,46]. From the NO-TPO profiles (Fig. 10), the potassium-containing catalysts show the lower activation temperature and higher abilities for NO oxidation to  $\text{NO}_2$ , especially for the 5KCo-NW catalyst. Therefore, the 5KCo-NW catalyst also displays the highest catalytic activity among these catalysts. Its catalytic activity of  $T_{10}$  (279 °C),  $T_{50}$  (324 °C) and  $S_{\text{CO}_2}$  (100%) is better than that of the noble metal Pt/ $\text{Al}_2\text{O}_3$  catalysts ( $T_{10} = 321$  °C,  $T_{50} = 384$  °C) under loose contact mode.

Combined the catalytic activities of the as-prepared catalysts in the  $\text{O}_2/\text{N}_2$  and  $\text{NO}/\text{O}_2/\text{N}_2$  atmosphere, the catalytic performance of the as-prepared catalysts with the different content of potassium follows the order of 5KCo-NW > 10KCo-NW > 1KCo-NW (Table 2), indicating that the optimal loading of potassium is 5%. For the 1KCo-NW catalyst containing less potassium, the active sites offered by potassium are in small quantity. Thus, the 1KCo-NW catalyst can not efficiently eliminate the soot particulates. As to the 10KCo-NW catalyst, the increased amount of potassium causes serious aggregation by forming the large  $\text{K}_2\text{CO}_3$  particles. The accumulation of  $\text{K}_2\text{CO}_3$  nanoparticles blocks the space among these  $\text{Co}_3\text{O}_4$  nanowires as displayed in the inset image in Fig. 3d1, and decreases the contact chance between the soot particulates and the catalyst. As a result, the 10KCo-NW catalyst shows relatively poor activity than the 5KCo-NW catalyst for catalytic soot combustion. As to the 5KCo-NW catalyst containing the appropriate potassium species, the  $\text{K}_2\text{CO}_3$  nanoparticles are uniformly distributed, and the open space among these  $\text{Co}_3\text{O}_4$  nanowires is well retained. The 5KCo-NW catalyst possesses the highest oxidation ability and the largest

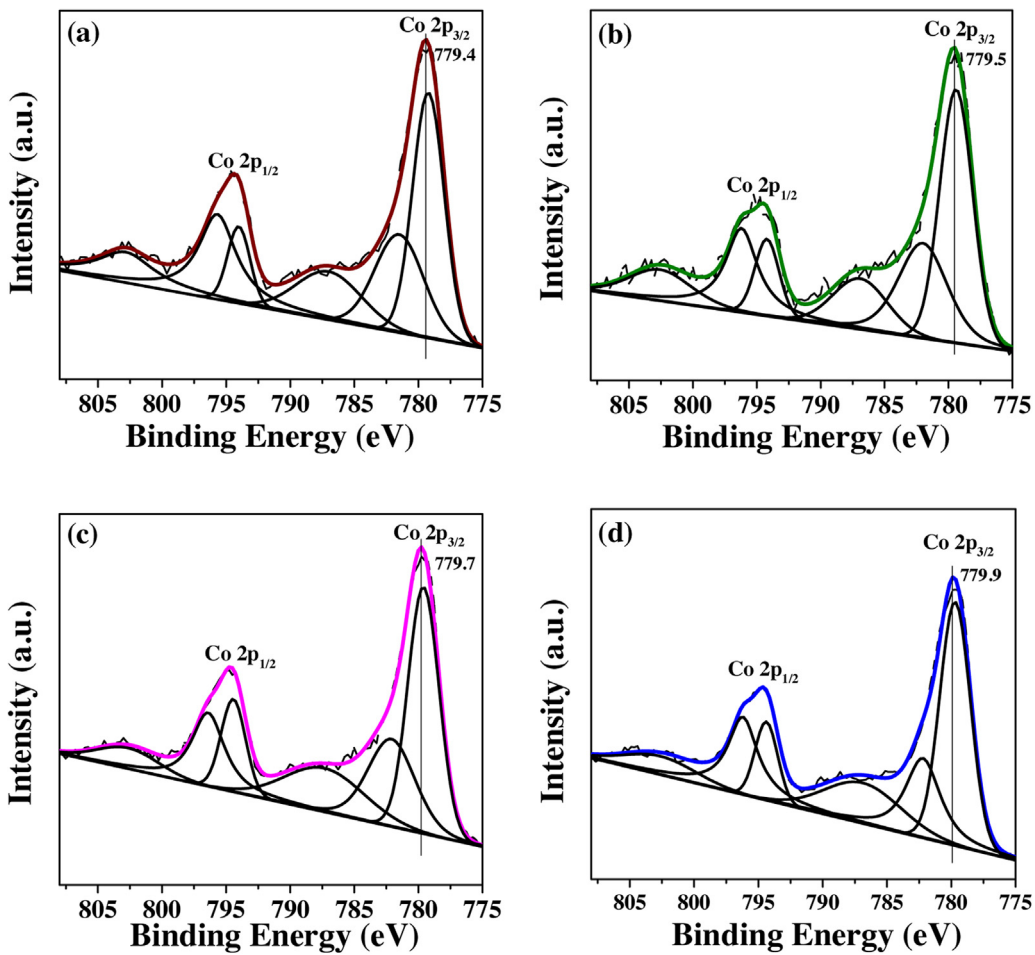


**Fig. 6.** XPS spectra of Co 2P of (a) 10KCo-NW, (b) 5KCo-NW, (c) 1KCo-NW and (d) Co-NW. The dash line is the experimental data, and the solid line is the peak fitting data.

**Table 3**

The specific reaction rate ( $R_s$ ), active oxygen ( $O^*$ ) amount and active oxygen density for soot combustion at 360 °C over the as-prepared catalysts under GCM.

Catalysts	$R_s$ ( $\text{mol s}^{-1} \text{m}^{-2} \times 10^{-9}$ )	$O^*$ amount ( $\text{mol g}^{-1} \times 10^{-5}$ )	$O^*$ density ( $\text{nm}^{-2}$ )
Co-NW	1.45	3.85	0.20
1KCo-NW	2.13	4.99	0.31
5KCo-NW	6.72	19.96	1.35
10KCo-NW	5.01	10.46	0.90

number of surface adsorbed oxygen species as well as the active oxygen species. Thus, the 5KCo-NW sample shows the best catalytic performance for soot oxidation. Interestingly, the catalytic activity order is in good accordance with the results of XPS and soot-TPR. So, these results are deduced that the surface adsorbed oxygen plays a key role in the process of soot oxidation.

### 3.2.2. Isothermal reaction

In order to achieve the specific reaction rate ( $R_s$ ) and the amounts of active oxygen ( $O^*$  amount), the isothermal reaction and isothermal anaerobic titrations were performed at 360 °C, as shown in Fig. S1, S2. Table 3 summarizes the calculated values of the specific reaction rate and the density of the active oxygen for soot oxidation. It indicates that loading of potassium promotes the catalytic soot combustion performance. On one hand, the interaction between potassium and  $\text{Co}_3\text{O}_4$  lowers the temperature of activating oxygen and improves the catalytic soot oxidation activity. On the other hand, the supported potassium increases the amounts of oxygen vacancies, which will accelerate the mobility of lattice oxy-

gen. During the process of isothermal anaerobic titrations, when the gaseous oxygen was cut off, the soot particulates can only be oxidized by the surface oxygen species existing on the catalysts. The amounts of active oxygen of the as-prepared catalysts are well in agreement with the results of XPS and catalytic activities for soot combustion, which further indicates that active oxygen is important for catalytic soot combustion over the xKCo-NW catalysts.

### 3.2.3. Effect of the active oxygen species

Since the catalytic activity for soot oxidation is closely related to the surface adsorbed oxygen species, how it works over those without potassium (Co-NW) and potassium-promoted (5KCo-NW) catalysts? Fig. 11 shows the result of the soot-TPO experiments in the different atmospheres ( $\text{N}_2$ , 600 ppm  $\text{NO}/\text{N}_2$ , 5%  $\text{O}_2/\text{N}_2$ , 5%  $\text{O}_2$ /600 ppm  $\text{NO}/\text{N}_2$ ) over the Co-NW and 5KCo-NW catalysts. Compared with the catalytic soot combustion performance in the  $\text{N}_2$  atmosphere, when  $\text{O}_2$  is introduced, the tiny peak becomes larger at the same temperature range (320–600 °C), indicating the increased soot combustion rate. The result implies that the gaseous oxygen could be easily activated on the same oxygen vacancies and converted into surface active oxygen species so that the soot combustion could take place continuously. The role of the active oxygen species has been further confirmed by isothermal anaerobic titrations (Fig. S2). The result shows that once the  $\text{O}_2$  flow was cut off, the soot combustion activity gradually decreased, confirming the participation of the active oxygen derived from the gaseous oxygen under the real reaction conditions. The addition of 600 ppm  $\text{NO}$  to pure  $\text{N}_2$  could not improve the catalytic soot oxidation performance. However, through introducing of 5%  $\text{O}_2$  to  $\text{NO}$ -including

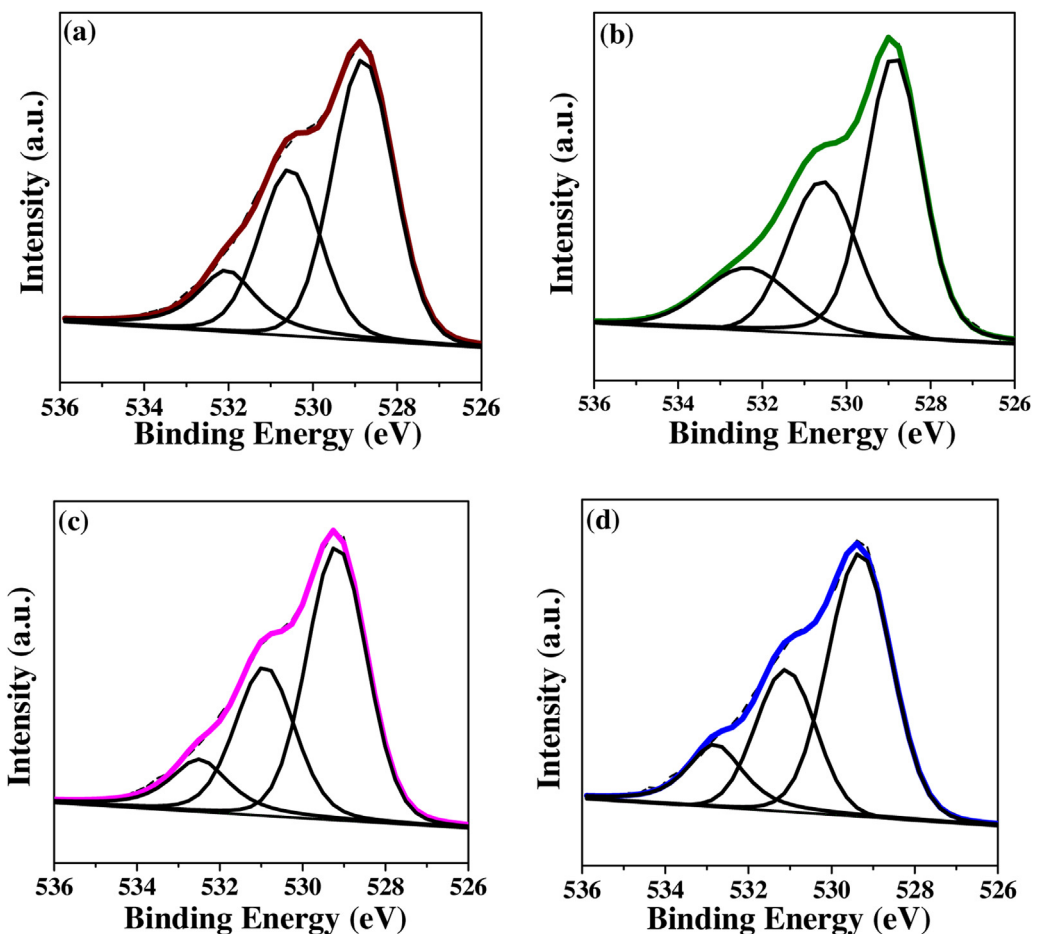


**Fig. 7.** XPS spectra of O 1s of (a) 10KCo-NW, (b) 5KCo-NW, (c) 1KCo-NW and (d) Co-NW. The dash line is the experimental data, and the solid line is the peak fitting data.

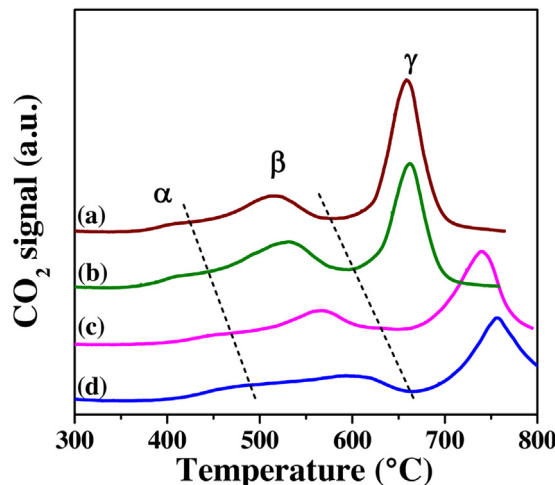


**Fig. 8.** Soot-TPR of the as-prepared catalysts: (a) 10KCo-NW, (b) 5KCo-NW, (c) 1KCo-NW and (d) Co-NW.

atmosphere can sharply lower the reaction temperature for soot oxidation, because NO can be oxidized to the active NO<sub>2</sub> over the Co-NW and 5KCo-NW catalysts. Thus, the preformed active NO<sub>2</sub> may act as the stronger oxidant, lowering the ignition temperature of soot combustion.

Compared with the catalytic activities of the Co-NW and 5KCo-NW catalysts, the potassium-containing catalyst always shows the higher catalytic performance and reaction rate in no matter what

the atmosphere. The high catalytic activity of the 5KCo-NW can be elucidated from several aspects: (1) K<sup>+</sup> can be used as an independent catalyst or active component of catalyst for soot oxidation and has a high catalytic performance [30]; (2) the interaction between potassium and Co<sub>3</sub>O<sub>4</sub> enhanced the oxidation ability of the 5KCo-NW catalyst and increased the number of surface adsorbed oxygen species (supported by the results of XPS and soot-TPR) [31]; (3) potassium species is a kind of molten salt, which can enhance the contact chance between catalysts and soot particulates by increasing surface mobility [30,47]; (4) the 5KCo-NW catalyst possesses the higher ability for NO oxidation to NO<sub>2</sub> than that of the Co-NW.

### 3.2.4. Effect of the trapped NO<sub>x</sub> species

Generally, NO<sub>x</sub> can be adsorbed and trapped in the form of chemisorbed NO<sub>x</sub> species and nitrate/nitrite on basic materials, such as potassium carbonate, under lean-burn conditions [48]. To reveal the influence of these trapped NO<sub>x</sub> species on the catalytic soot combustion process, the soot-TPO experiments were performed over the 5KCo-NW sample under different conditions. For comparison, the 5KCo-NW catalyst was pretreated in NO/O<sub>2</sub> at 350 °C to completely trap NO<sub>x</sub> to reach a saturated state, and the corresponding catalyst is named as 5KCo-NW-S. Fig. S5 shows the NO<sub>x</sub>-TPD profile of the 5KCo-NW-S catalyst. In Fig. S5, the sharp NO<sub>x</sub> desorption peak centered at around 190 °C corresponds to the chemisorbed NO<sub>x</sub> species, while the peak in the region of 250–450 °C originates from the decomposition of the formed nitrates/nitrites species [49].

Fig. 12 displays the results of the soot-TPO experiments over the 5KCo-NW and 5KCo-NW-S catalysts under the different conditions.

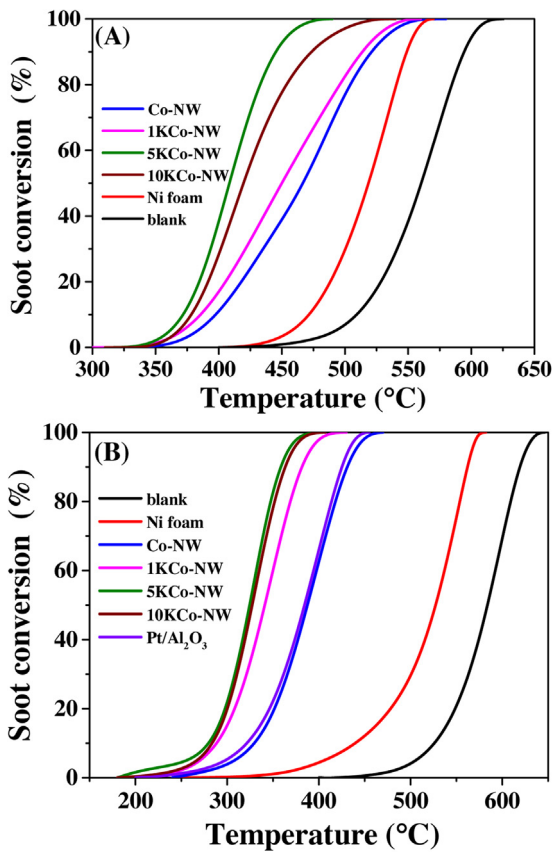


**Fig. 9.** Soot catalytic combustion activity of the as-prepared catalysts in (A) 5% O<sub>2</sub> balanced by N<sub>2</sub> and (B) 600 ppm NO and 5% O<sub>2</sub> balanced by N<sub>2</sub> under loose contact mode.

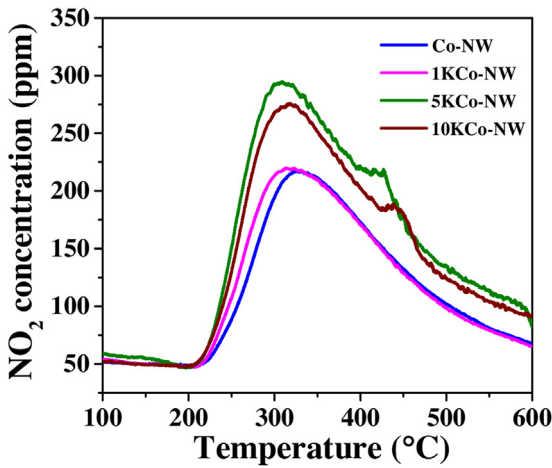


**Fig. 10.** The profiles for NO oxidation to NO<sub>2</sub> over the as-prepared catalysts in the NO/O<sub>2</sub>/N<sub>2</sub> atmosphere.

In Fig. 12a, only one CO<sub>2</sub> peak centered at around 400 °C appears for soot combustion over the 5KCo-NW sample in the O<sub>2</sub>/N<sub>2</sub> atmosphere. It is ascribed to soot combustion with the active oxygen species on the catalyst. In Fig. 12b, the CO<sub>2</sub> shoulder peaks for soot oxidation over the 5KCo-NW in the NO/O<sub>2</sub>/N<sub>2</sub> atmosphere center at 224 °C (weak peak), and 329 °C (strong peak). The peak locating at the low temperature (below 300 °C) is denoted as LT peak, and the peak locating at the high temperature (above 300 °C) is denoted as HT peak. Fig. 12c and d display the CO<sub>2</sub> peaks for soot combustion in the N<sub>2</sub> atmosphere over the 5KCo-NW-S and 5KCO-NW catalysts, respectively. In Fig. 12c, for the 5KCo-NW-S catalyst

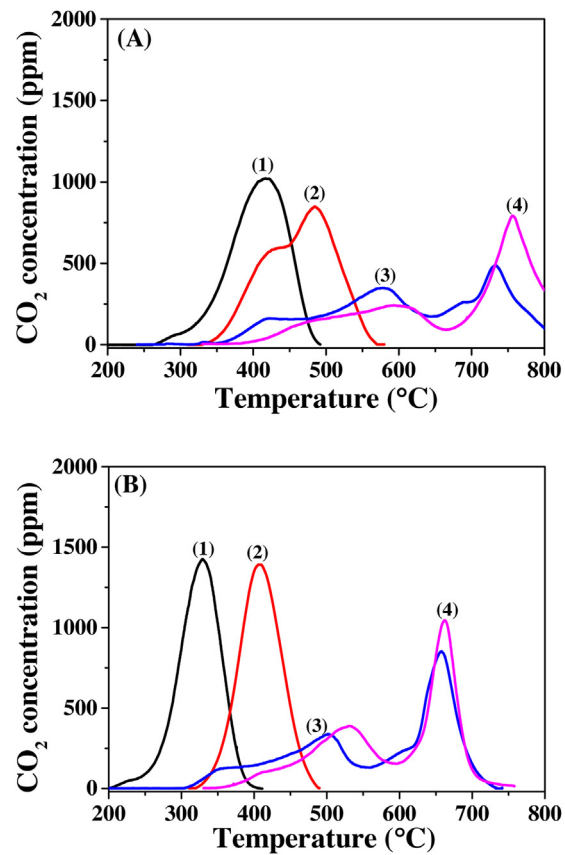


**Fig. 11.** The CO<sub>2</sub> concentration curves during the soot-TPO reaction over Co-NW (A) and 5 K Co-NW (B) in different atmospheres: (1) 600 ppm NO/5% O<sub>2</sub>/N<sub>2</sub>, (2) 5% O<sub>2</sub>/N<sub>2</sub>, (3) 600 ppm NO/N<sub>2</sub> and (4) N<sub>2</sub>.

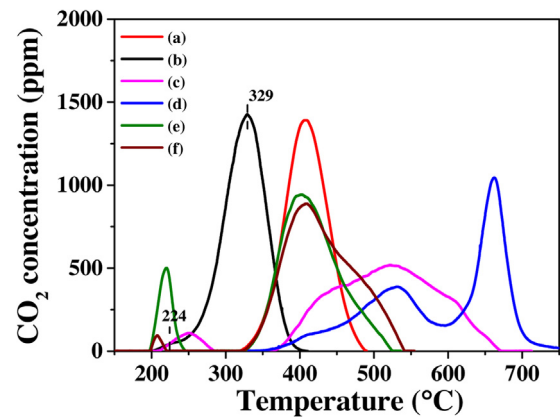


**Fig. 12.** The CO<sub>2</sub> concentration in the soot-TPO process: (a) over the 5KCo-NW in the O<sub>2</sub>/N<sub>2</sub> atmosphere, (b) over the 5KCo-NW in the NO/O<sub>2</sub>/N<sub>2</sub> atmosphere, (c) over the 5KCo-NW-S in the N<sub>2</sub> atmosphere, (d) over the 5KCo-NW in the N<sub>2</sub> atmosphere, (e) over the 5KCo-NW-S in the O<sub>2</sub>/N<sub>2</sub> atmosphere, and (f) over the 5KCo-NW-S, pretreated in N<sub>2</sub> for 30 min at 190 °C, in the O<sub>2</sub>/N<sub>2</sub> atmosphere.

the LT weak CO<sub>2</sub> peak locates at 200–280 °C, whereas the broad and strong HT CO<sub>2</sub> peak appears at above 350 °C. The HT peak could be ascribed to soot combustion with the active oxygen species, probably as well as the stored nitrate/nitrite species. In Fig. 12d, only HT CO<sub>2</sub> peaks appear, and soot oxidation starts from about 350 °C over the 5KCO-NW catalyst without the aid of O<sub>2</sub> and/or NO<sub>x</sub>. Herein, the HT peak below 600 °C could be attributed to soot combustion with the surface active oxygen, while the HT peak above 600 °C could correspond to soot combustion with the bulk lattice oxygen. Interestingly, the LT CO<sub>2</sub> peak in Fig. 12c is very close to the LT peak in

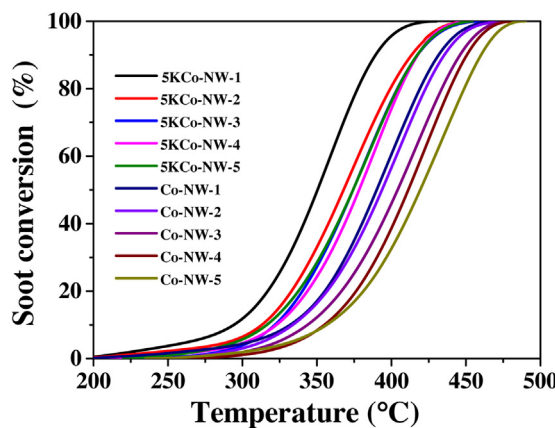


**Fig. 13.** The five cycles soot-TPO in 600 ppm NO and 5% O<sub>2</sub> balanced by N<sub>2</sub> over the 5KCo-NW and Co-NW catalysts.

**Fig. 12b.** Thus, we propose that the LT CO<sub>2</sub> peak in **Fig. 12b**, as well as in **Fig. 12c**, is related to soot combustion with the chemisorbed NO<sub>x</sub> species on the catalysts; while the strong HT peak in **Fig. 12b** belongs to soot combustion with the gaseous NO<sub>2</sub>, originated from NO oxidation over the 5KCO-NW catalyst in the NO/O<sub>2</sub> atmosphere. It illustrates that for soot combustion the chemisorbed NO<sub>x</sub> species on the 5KCO-NW catalyst are more active than the gaseous NO<sub>2</sub>. Additionally, it also indicates that in the absence of O<sub>2</sub>, the stored nitrate/nitrite species are more active than the bulk lattice oxygen after comparison of the HT peaks in **Fig. 12c** and **d**.

In **Fig. 12e**, in the O<sub>2</sub>/N<sub>2</sub> atmosphere, the LT CO<sub>2</sub> peak, resulting from the chemisorbed NO<sub>x</sub> species for soot combustion over the 5KCo-NW-S, becomes stronger and sharper than that in the N<sub>2</sub> atmosphere at 200–250 °C in **Fig. 12c**. It indicates that the presence of O<sub>2</sub> can further accelerate the soot combustion rate with the chemisorbed NO<sub>x</sub> species. **Fig. S5** shows that the desorption peak of the chemisorbed NO<sub>x</sub> species centers at around 190 °C. To confirm our assumption, we purge the 5KCO-NW-S catalyst in the N<sub>2</sub> flow at 190 °C for 30 min to desorb the chemisorbed NO<sub>x</sub>, at which soot combustion does not happen yet (<200 °C). Thereafter, the soot-TPO experiment is carried out over the 5KCO-NW-S catalyst in the N<sub>2</sub> flow. Obviously, in **Fig. 12f**, the LT CO<sub>2</sub> peak, resulting from the remained tiny amount of the chemisorbed NO<sub>x</sub>, seriously weakens. Accordingly, it confirms our assumption that the LT CO<sub>2</sub> peak is originated from soot combustion with the chemisorbed NO<sub>x</sub> species. Interestingly, the HT CO<sub>2</sub> peak in **Fig. 12e** and **f** is similar with that in **Fig. 12a**, which corresponds to soot combustion with the active oxygen species over the 5KCo-NW catalyst in the O<sub>2</sub>/N<sub>2</sub> atmosphere. As shown in **Fig. S5**, the formed nitrate/nitrite species on the 5KCo-NW-S catalyst decomposes at above 250 °C. Combining with the decomposition temperature range of the nitrate/nitrite species in **Fig. S5** and the temperature range of the HT CO<sub>2</sub> peak in **Fig. 12a**, **e** and **f**, we can draw a conclusion that the stored nitrate/nitrite species are catalytically inert in the O<sub>2</sub> atmosphere for soot oxidation under the gravitation contact mode.

In summary: (1) the chemisorbed NO<sub>x</sub> species play an important role in the soot ignition process; (2) the chemisorbed NO<sub>x</sub> species are more active than the gaseous NO<sub>2</sub>; (3) the gaseous oxygen can accelerate soot combustion with the chemisorbed NO<sub>x</sub> species; (4) the stored nitrate/nitrite species are catalytically inert in the presence of O<sub>2</sub> for soot combustion under GCM.

### 3.2.5. The stability of the as-prepared catalysts

To investigate the stability of the as-prepared catalysts, five consecutive cycles of soot combustion were carried out over the 5KCo-NW and Co-NW catalysts in 600 ppm NO and 5% O<sub>2</sub> balanced by N<sub>2</sub>. **Fig. 13** shows the results of the five consecutive cycles of

**Table 4**

The BE of Co 2p<sub>3/2</sub> and the K/Co atomic ratios of the used catalysts after several soot-TPO cycles.

Catalysts	Co 2p <sub>3/2</sub> (eV)	K/Co
Co-NW-5	779.9	–
5KCo-NW-1	779.5	0.050
5KCo-NW-2	779.5	0.049
5KCo-NW-3	779.5	0.047
5KCo-NW-4	779.5	0.048

soot-TPO over the Co-NW and 5KCo-NW. For the Co-NW catalyst, the catalytic performance gradually decreases in the followed cycle. Probably, it is because the particle size of Co<sub>3</sub>O<sub>4</sub> becomes larger after the five consecutive cycles of soot-TPO, as observed from the SEM images (**Fig. 14**). After introducing potassium, the catalytic performance of the catalyst decreases in the second cycle and then gets stable in the followed cycles, and the performances of the 5KCo-NW catalyst in the five consecutive cycles of soot-TPO experiment are always better than that of the Co-NW catalyst. The content of potassium in the 5KCo-NW after the five consecutive cycles of soot-TPO decreases from 5% to 1.7%, as measured by ICP. From **Fig. S6** and **Table 4**, the Co 2p<sub>3/2</sub> peak of the used 5KCo-NW after the five consecutive cycles of soot-TPO still shifts to lower binding energies, which is similar to the results of the fresh catalyst. It indicates that the interaction between K and Co is still maintained. Additionally, the K/Co ratio of the 5KCo-NW decreases from 0.105 to 0.050 in the second cycle, and then keeps constant after several soot combustion cycles. Thus, we suppose that there are two types of potassium species, most potassium species is in the form of separate phases and few interacts with cobalt oxide. The segregated potassium species is lost during the second soot combustion cycle, and that the potassium interacted with cobalt oxide remains on the catalyst affecting the behavior of the Co<sup>2+</sup>/Co<sup>3+</sup> redox cycle. Moreover, the particle size of Co<sub>3</sub>O<sub>4</sub> in the 5KCo-NW catalyst after the five consecutive cycles of soot-TPO has little change. Thus, the catalytic performance of the catalyst decreases in the second cycle because of loss of the segregated potassium, and then gets stable in the followed cycles. These results demonstrate that the stabilized potassium species through interaction with Co<sub>3</sub>O<sub>4</sub> can promote the catalytic activity for soot combustion. The effect of water vapor on the catalytic activity for soot oxidation over the 5KCo-NW catalyst was confirmed by introducing 5% H<sub>2</sub>O to 600 ppm NO and 5% O<sub>2</sub> balanced by N<sub>2</sub> atmosphere during soot-TPO test. As shown in **Fig. S7**, the reaction rate of soot oxidation in the presence of 5% H<sub>2</sub>O is slightly faster than that in the absence of H<sub>2</sub>O, in accordance with the previous reports [50–53]. Thus, these results certify the high stability and water resistance of the 5KCo-NW catalyst in the soot combustion reaction.

In order to further confirm the effect of the trapped NO<sub>x</sub> species, we also performed the soot-TPO experiments over the used 5KCo-NW sample after the five soot-TPO cycles under different conditions, as shown in **Fig. 15**. Firstly, the used 5KCo-NW catalyst after the five soot-TPO cycles was saturated in mixture gas consisting of 400 ppm of NO, 5% O<sub>2</sub> and balance N<sub>2</sub> at 350 °C for NO<sub>x</sub> chemisorption before the soot-TPO experiment, and the sample is denoted as 5KCo-NW-used-S. The NO<sub>x</sub>-TPD was performed over the 5KCo-NW-used-S sample, and the other experimental conditions were the same with the NO<sub>x</sub>-TPD over the 5KCo-NW-S, as shown in **Fig. S5**. Compared with the NO<sub>x</sub>-TPD over the 5KCo-NW-S catalyst, the amounts of the chemisorbed NO<sub>x</sub> species and the formed nitrates/nitrites species decrease due to the loss of part of potassium species in the process of soot combustion. For soot combustion over the 5KCo-NW-used-S, similarly to the results over the fresh catalyst, there are still two peaks: the low temperature (LT) peak at 200–250 °C and the high temperature (HT) peak at 320–550 °C. Compared with the fresh catalyst, the intensity of the

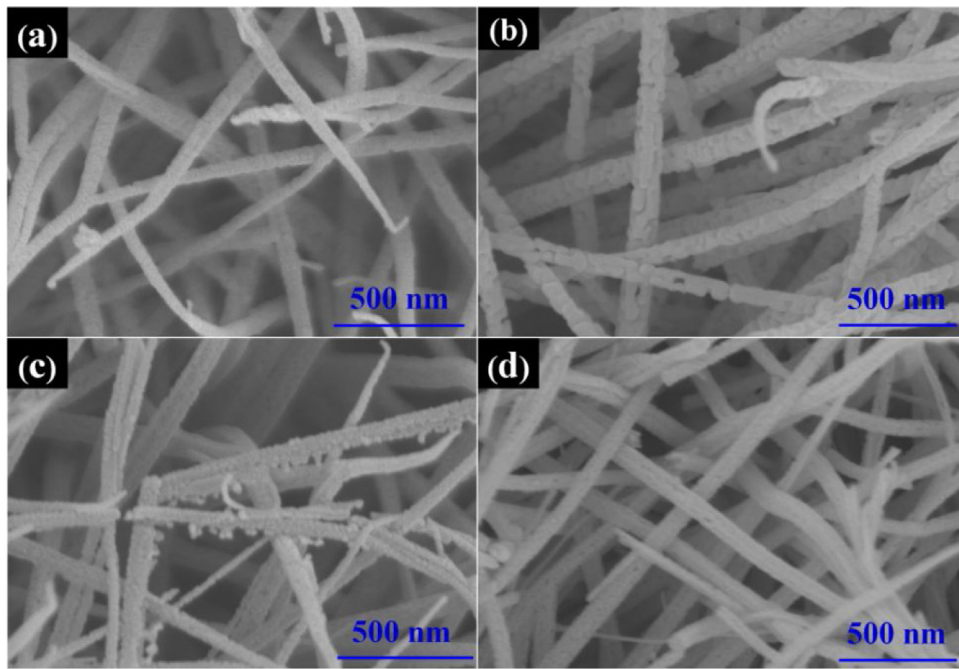


**Fig. 14.** SEM images of the different catalysts: (a) the fresh Co-NW, (b) the used Co-NW after the five consecutive soot-TPO cycles, (c) the fresh 5KCo-NW and (d) the used 5KCo-NW after the five consecutive soot-TPO cycles.

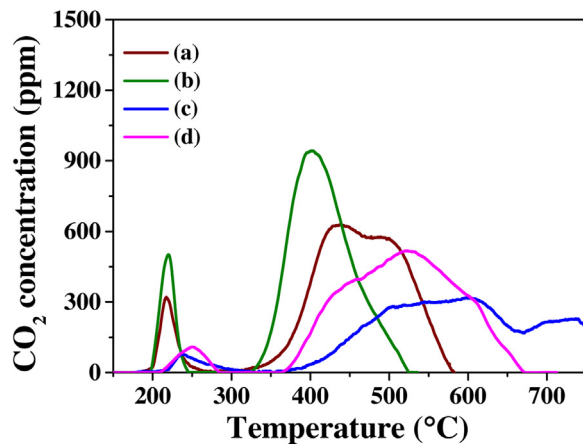


**Fig. 15.** The CO<sub>2</sub> concentration in the soot-TPO process: (a) over the 5KCo-NW-used-S in the O<sub>2</sub>/N<sub>2</sub> atmosphere, (b) over the 5KCo-NW-S in the O<sub>2</sub>/N<sub>2</sub> atmosphere, (c) over the 5KCo-NW-used-S in the N<sub>2</sub> atmosphere and (d) over the 5KCo-NW-S in the N<sub>2</sub> atmosphere.

LT peaks decreases, and the HT peaks shift to the higher temperature, because of loss of part of potassium species. The results of the soot-TPO over the 5KCo-NW-used-S sample are similar to those over the fresh 5KCo-NW catalyst.

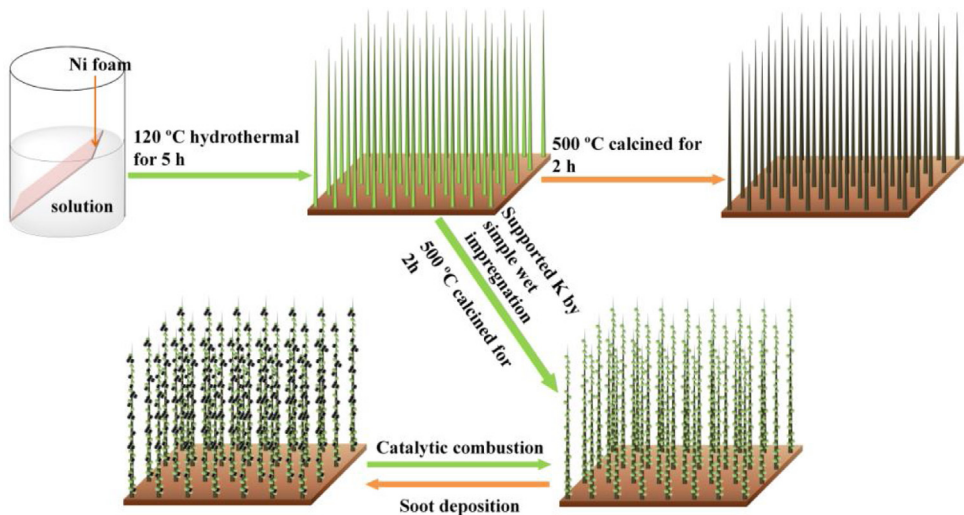
### 3.2.6. Mechanism consideration

Based on the above results and analysis, **Scheme 1** describes the pathway of the catalyst preparation and soot oxidation over the xKCo-NW catalysts, which is consisted of five steps: (1) to synthesize the precursor of the Co-NW catalyst through the hydrothermal process at 120 °C for 5 h [34]; (2) the Co-NW catalyst was obtained through calcining the precursor at 500 °C for 2 h; (3) Through a facile wet impregnation, potassium was supported on the precursor of the Co-NW, and the precursors with potassium were calcined to obtain the xKCo-NW catalysts; (4) the xKCo-NW catalysts and the soot particulates were mixed through dropping the ethanol suspension with soot particulates to meet the loose contact condition,

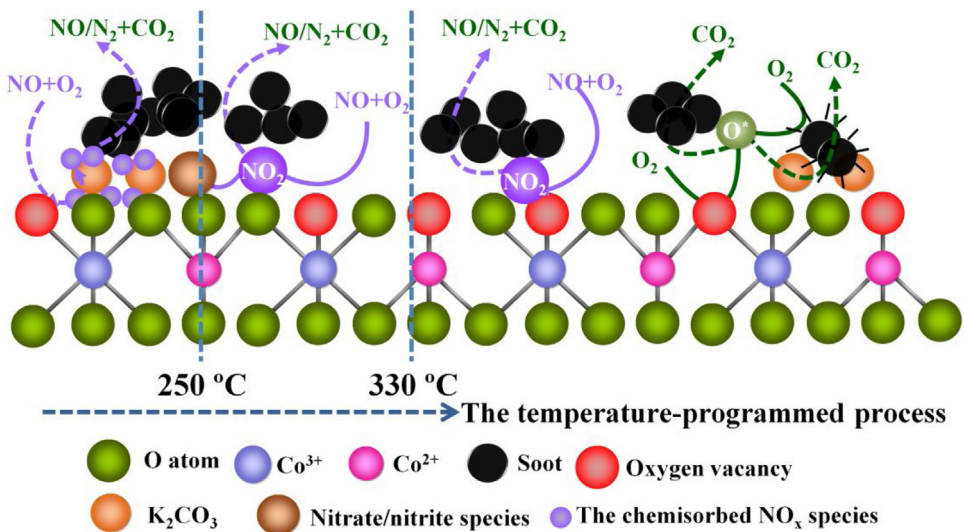
and the SEM image (Fig. S8) exhibits the contact situation between the 5KCo-NW and the soot particulates under the gravitation contact mode; (5) the soot particulates were catalytically oxidized by the active oxygen species of the xKCo-NW catalyst and NO<sub>2</sub> derived from the NO oxidation; meanwhile the catalysts simultaneously obtained regeneration. The catalytic soot oxidation mechanism will be described in details in the next section.

In the O<sub>2</sub>/N<sub>2</sub> atmosphere, catalytic soot oxidation over the potassium-including catalysts follows the oxygen spillover mechanism. The electron-donor effect of potassium can change the  $\pi$  electrons distribution of soot, and thus, electrons with higher energy states aggregate on the surface of soot particulate, which strengthens the driving force for efficient electron transfer from soot to O<sub>2</sub> [54–57]. For the loose contact mode between soot particulates and catalysts, the oxygen spillover mechanism greatly promotes the catalytic soot combustion performance.

In the NO/O<sub>2</sub>/N<sub>2</sub> atmosphere, the process of the NO<sub>x</sub>-aided catalytic soot combustion is comparatively complex, because potassium can adsorb and store NO<sub>x</sub> to form the chemisorbed NO<sub>x</sub> species and the nitrate/nitrite species on the catalysts. Our results show that in the presence of O<sub>2</sub>, only the chemisorbed NO<sub>x</sub> species involves in soot combustion, while the formed nitrate/nitrite can not promote catalytic soot combustion under GCM. Therefore, the reaction pathway for soot oxidation over the xKCo-NW catalysts can be partitioned into three sections at different temperatures, as shown in **Scheme 2**. In the temperature-programmed process (100–200 °C), NO is adsorbed and then oxidized by the active oxygen, forming the chemisorbed NO<sub>x</sub> species and/or the nitrate/nitrite on the surface of the catalysts, as well as the gaseous NO<sub>2</sub>. When the temperature reaches ~200 °C, the soot particulates are oxidized by the chemisorbed NO<sub>x</sub> species. At above 250 °C, the chemisorbed NO<sub>x</sub> species completely desorb from the surface of the catalysts; meanwhile the soot particulates are mainly oxidized by the gaseous NO<sub>2</sub>. At above 330 °C, the active oxygen species on the catalysts start to react with soot particulates. Therefore, at the relatively high temperatures the soot particulates are mainly oxidized by the active oxygen species following the oxygen spillover mechanism and the gaseous NO<sub>2</sub>.



**Scheme 1.** A schematic diagram describes the synthesis of the xKCo-NW catalysts and the process for the catalytic soot oxidation.



**Scheme 2.** Illustration of reaction mechanisms for soot combustion over the xKCo-NW catalysts under GCM.

#### 4. Conclusion

Summarily, we synthesize a series of potassium-promoted  $\text{Co}_3\text{O}_4$  nanowires supported on the monolithic 3-DM nickel foam substrate through a facile hydrothermal and impregnation method. The as-prepared catalysts show excellent catalytic soot oxidation performance under GCM. The 3-DM structure of Ni foam and the space among these nanowires can greatly increase the amount of contact sites between catalysts and soot particulates. After introducing potassium, the performance for catalytic soot oxidation was further improved, especially over the 5KCo-NW. Combined with the results of characterizations and catalytic performance, for soot oxidation over the potassium-promoted catalysts, the following several conclusions can be summarized: (1) the load of potassium provides the new active sites, increases the surface absorbed oxygen species and lowers the temperature for NO oxidation to  $\text{NO}_2$ ; (2) the 5KCo-NW catalyst displays the highest catalytic activity of  $T_{10}$  ( $279^\circ\text{C}$ ),  $T_{50}$  ( $324^\circ\text{C}$ ) and  $S_{\text{CO}_2}$  (100%) among these catalysts; (3) two types of potassium species exist in the catalysts: most potassium species is in the form of separate phases, and few interacts with cobalt oxide. The interaction between potassium species and cobalt oxide stabilizes a part of potassium species, and thus

improve the catalytic stability of the catalyst for soot combustion; (4) the gaseous  $\text{NO}_2$  and the chemisorbed  $\text{NO}_x$  on the catalyst are the active species for soot combustion; (5) the chemisorbed  $\text{NO}_x$  species are more active than the gaseous  $\text{NO}_2$ , and the presence of  $\text{O}_2$  can accelerate soot combustion with the chemisorbed  $\text{NO}_x$  species; (6) under GCM, in the presence of  $\text{O}_2$  the stored nitrate/nitrite species on the catalysts are catalytically inert for soot oxidation; whereas in the absence of  $\text{O}_2$ , the stored nitrate/nitrite species on the catalysts can involve in soot combustion at high temperatures. Our work provides a new insight to design the effective catalytic systems upon catalytic soot combustion.

#### Acknowledgements

We are grateful to the National Natural Science Foundation of China (Nos. 21476159, U1232118), the Program of Introducing Talents of Discipline to China Universities (No. B06006), the 973 program (2014CB932403), and the Natural Science Foundation of Tianjin, PR China (15JCZDJC37400, 15JCYJC23000). Thanks to Beijing Synchrotron Radiation Facility (Chinese Academy of Sciences) for the assistance with XAFS measurements.

## Appendix A. Supplementary data

Supplementary data associated with this article can be found, in the online version, at <http://dx.doi.org/10.1016/j.apcatb.2017.06.035>.

The isothermal reaction and isothermal anaerobic titrations, electron microscope characterization on the Ni foam, the specific surface area,  $\text{CO}_2$ -TPD,  $\text{NO}_x$ -TPD, the XPS Co 2p of the spent catalyst, the effect of  $\text{H}_2\text{O}$  on soot combustion performance over the 5KCo-NW catalyst and the images of the contact situation between soot particulates and the 5KCo-NW catalyst under GCM.

## References

[1] M. Cortés-Reyes, C. Herrera, M.Á. Larrubia, L.J. Alemany, Intrinsic reactivity analysis of soot removal in LNT-catalysts, *Appl. Catal. B* 193 (2016) 110–120.

[2] C. Lee, Y. Jeon, S. Hata, J.P. Park, R. Akiyoshi, H. Saito, Y. Teraoka, Y.G. Shul, H. Einaga, Three-dimensional arrangements of perovskite-type oxide nano-fiber webs for effective soot oxidation, *Appl. Catal. B* 191 (2016) 157–164.

[3] N.D. Wasalathanthri, T.M. SantaMaria, D.A. Kriz, S.L. Dissanayake, C.H. Kuo, S. Biswas, S.L. Suib, Mesoporous manganese oxides for  $\text{NO}_2$  assisted catalytic soot oxidation, *Appl. Catal. B* 201 (2017) 543–551.

[4] R. Kimura, J. Wakabayashi, S.P. Elangovan, M. Ogura, T. Okubo, Nepheline from  $\text{K}_2\text{CO}_3$ /nanosized sodalite as a prospective candidate for diesel soot combustion, *J. Am. Chem. Soc.* 130 (2008) 12844–12845.

[5] R. Matarrese, S. Morandi, L. Castoldi, P. Villa, L. Lietti, Removal of  $\text{NO}_x$  and soot over  $\text{Ce}/\text{Zr}/\text{K}/\text{Me}$  ( $\text{Me} = \text{Fe}, \text{Pt}, \text{Ru}, \text{Au}$ ) oxide catalysts, *Appl. Catal. B* 201 (2017) 318–330.

[6] T. Andana, M. Piumetti, S. Bensaid, N. Russo, D. Fino, R. Pirone, Nanostructured ceria-praseodymium catalysts for diesel soot combustion, *Appl. Catal. B* 197 (2016) 125–137.

[7] Y.F. Yu, J.L. Ren, D.S. Liu, M. Meng, Domain-confined multiple collision enhanced catalytic soot combustion over a  $\text{Fe}_2\text{O}_3/\text{TiO}_2$ -nanotube array catalyst prepared by light-assisted cyclic magnetic adsorption, *ACS Catal.* 4 (2014) 934–941.

[8] T. Andana, M. Piumetti, S. Bensaid, L. Veyre, C. Thieuleux, N. Russo, D. Fino, E.A. Quadrelli, R. Pirone, Ceria-supported small Pt and Pt3Sn nanoparticles for  $\text{NO}_x$ -assisted soot oxidation, *Appl. Catal. B* 209 (2017) 295–310.

[9] G. Corro, S. Cebada, U. Pal, J.L.G. Fierro,  $\text{Au}^0-\text{Au}^{3+}$  bifunctional site mediated enhanced catalytic activity of  $\text{Au}/\text{ZnO}$  composite in diesel particulate matter oxidation, *J. Catal.* 347 (2017) 148–156.

[10] G. Corro, S. Cebada, U. Pal, J.L.G. Fierro, J. Alvarado, Hydrogen-reduced  $\text{Cu}/\text{ZnO}$  composite as efficient reusable catalyst for diesel particulate matter oxidation, *Appl. Catal. B* 165 (2015) 555–565.

[11] G. Corro, U. Pal, E. Ayala, E. Vidal, Diesel soot oxidation over silver-loaded  $\text{SiO}_2$  catalysts, *Catal. Today* 212 (2013) 63–69.

[12] X.D. Wu, F. Lin, D. Wang, J. Li, Simultaneous removal of soot and  $\text{NO}$  over thermal stable  $\text{Cu}-\text{Ce}-\text{Al}$  mixed oxides, *Catal. Commun.* 9 (2008) 2428–2432.

[13] P.G. Harrison, I.K. Ball, W. Daniell, P. Lukinskas, M. Céspedes, E.E. Miró, M.A. Ulla, Cobalt catalysts for the oxidation of diesel soot particulate, *Chem. Eng. J.* 95 (2003) 47–55.

[14] V. Rico-Pérez, E. Aneggi, A. Bueno-López, A. Trovarelli, Synergic effect of  $\text{Cu}/\text{Ce}_{0.5}\text{Pr}_{0.5}\text{O}_{2-\delta}$  and  $\text{Ce}_{0.5}\text{Pr}_{0.5}\text{O}_{2-\delta}$  in soot combustion, *Appl. Catal. B* 197 (2016) 95–104.

[15] G.Z. Zhang, Z. Zhao, J. Liu, G.Y. Jiang, A.J. Duan, J.X. Zheng, S.L. Chen, R.X. Zhou, Three dimensionally ordered macroporous  $\text{Ce}_{1-x}\text{Zr}_x\text{O}_2$  solid solutions for diesel soot combustion, *Chem. Commun.* 46 (2010) 457–459.

[16] L. Wang, S.Q. Fang, N.J. Feng, H. Wan, G. Guan, Efficient catalytic removal of diesel soot over Mg substituted  $\text{K}/\text{La}_{0.8}\text{Ce}_{0.2}\text{CoO}_3$  perovskites with large surface areas, *Chem. Eng. J.* 293 (2016) 68–74.

[17] Q. Wang, J.S. Chung, Z.H. Guo, Promoted soot oxidation by doped  $\text{K}_2\text{Ti}_2\text{O}_5$  catalysts and NO oxidation catalysts, *Ind. Eng. Chem. Res.* 50 (2011) 8384–8388.

[18] Q. Li, M. Meng, F.F. Dai, Y.Q. Zha, Y.N. Xie, T.D. Hu, J. Zhang, Multifunctional hydrotalcite-derived  $\text{K}/\text{MnMgAlO}$  catalysts used for soot combustion,  $\text{NO}_x$  storage and simultaneous soot- $\text{NO}_x$  removal, *Chem. Eng. J.* 184 (2012) 106–112.

[19] D. Fino, N. Russo, G. Saracco, V. Specchia, The role of suprafacial oxygen in some perovskites for the catalytic combustion of soot, *J. Catal.* 217 (2003) 367–375.

[20] D. Fino, N. Russo, C. Badini, G. Saracco, V. Specchia, Effect of active species mobility on soot-combustion over Cs-V catalysts, *AIChE J.* 49 (2003) 2173–2180.

[21] J. Liu, Z. Zhao, J.Q. Wang, C.M. Xu, A. Duan, G.Y. Jiang, Q. Yang, The highly active catalysts of nanometric  $\text{CeO}_2$ -supported cobalt oxides for soot combustion, *Appl. Catal. B* 84 (2008) 185–195.

[22] Y.C. Wei, J. Liu, Z. Zhao, Y.S. Chen, C.M. Xu, A.J. Duan, G.Y. Jiang, H. He, Highly active catalysts of gold nanoparticles supported on three-dimensionally ordered macroporous  $\text{LaFeO}_3$  for soot oxidation, *Angew. Chem. Int. Ed.* 50 (2011) 2326–2329.

[23] Y.C. Wei, J. Liu, Z. Zhao, A.J. Duan, G.Y. Jiang, C.M. Xu, J.S. Gao, H. He, X.P. Wang, Three-dimensionally ordered macroporous  $\text{Ce}_{0.8}\text{Zr}_{0.2}\text{O}_2$ -supported gold nanoparticles: synthesis with controllable size and super-catalytic performance for soot oxidation, *Energy Environ. Sci.* 4 (2011) 2959–2970.

[24] J.L. Ren, Y.F. Yu, F.F. Dai, M. Meng, J. Zhang, L.R. Zheng, T.D. Hu, Domain-confined catalytic soot combustion over  $\text{Co}_3\text{O}_4$  anchored on a  $\text{TiO}_2$  nanotube array catalyst prepared by mercaptoacetic acid induced surface-grafting, *Nanoscale* 5 (2013) 12144–12149.

[25] M.E. Gálvez, S. Ascaso, P. Stelmachowski, P. Legutko, A. Kotarba, R. Moliner, M.J. Lázaro, Influence of the surface potassium species in  $\text{Fe}/\text{Al}_2\text{O}_3$  catalysts on the soot oxidation activity in the presence of  $\text{NO}_x$ , *Appl. Catal. B* 152–153 (2014) 88–98.

[26] R. Matarrese, L. Castoldi, N. Artioli, E. Finocchio, G. Busca, L. Lietti, On the activity and stability of  $\text{Pt}-\text{K}/\text{Al}_2\text{O}_3$  LNT catalysts for diesel soot and  $\text{NO}_x$  abatement, *Appl. Catal. B* 144 (2014) 783–791.

[27] C.M. Cao, X.G. Li, Y.Q. Zha, J. Zhang, T.D. Hu, M. Meng, Crossed ferric oxide nanosheets supported cobalt oxide on 3-dimensional macroporous Ni foam substrate used for diesel soot elimination under self-capture contact mode, *Nanoscale* 8 (2016) 5857–5864.

[28] Y.F. Yu, M. Meng, F.F. Dai, The monolithic lawn-like  $\text{CuO}$ -based nanorods array used for diesel soot combustion under gravitational contact mode, *Nanoscale* 5 (2013) 904–909.

[29] C.M. Cao, Y.X. Zhang, D.S. Liu, M. Meng, Gravity-driven multiple collision-enhanced catalytic soot combustion over a space-open array catalyst consisting of ultrathin ceria nanobelts, *Small* 11 (2015) 3659–3664.

[30] H.M. An, P.J. McGinn, Catalytic behavior of potassium containing compounds for diesel soot combustion, *Appl. Catal. B* 62 (2006) 46–56.

[31] Q. Li, M. Meng, N. Tsubaki, X.G. Li, Z.Q. Li, Y.N. Xie, T.D. Hu, J. Zhang, Performance of K-promoted hydrotalcite-derived  $\text{CoMgAlO}$  catalysts used for soot combustion,  $\text{NO}_x$  storage and simultaneous soot- $\text{NO}_x$  removal, *Appl. Catal. B* 91 (2009) 406–415.

[32] R. Matarrese, L. Castoldi, L. Lietti, Reaction between soot and stored  $\text{NO}_x$  over K-based LNT catalysts investigated by temperature programmed methods and labeling isotopic experiments, *Catal. Today* 197 (2012) 228–235.

[33] R. Matarrese, N. Artioli, L. Castoldi, L. Lietti, P. Forzatti, Interaction between soot and stored  $\text{NO}_x$  during operation of LNT  $\text{Pt}-\text{Ba}/\text{Al}_2\text{O}_3$  catalysts, *Catal. Today* 184 (2012) 271–278.

[34] J. Jiang, J.P. Liu, X.T. Huang, Y.Y. Li, R.M. Ding, X.X. Ji, Y.Y. Hu, Q.B. Chi, Z.H. Zhu, General synthesis of large-scale arrays of one-dimensional nanostructured  $\text{Co}_3\text{O}_4$  directly on heterogeneous substrates, *Cryst. Growth Des.* 10 (2010) 70–75.

[35] C.M. Cao, L.L. Xing, Y.X. Yand, Y. Tian, T. Ding, J. Zhang, T.D. Hu, L.R. Zheng, X.G. Li, The monolithic transition metal oxide crossed nanosheets used for diesel soot combustion under gravitational contact mode, *Appl. Surf. Sci.* 406 (2017) 245–253.

[36] Z.L. Zhang, D. Han, S.J. Wei, Y.X. Zhang, Determination of active site densities and mechanisms for soot combustion with  $\text{O}_2$  on Fe-doped  $\text{CeO}_2$  mixed oxides, *J. Catal.* 276 (2010) 16–23.

[37] Q.S. Liu, Z. Yan, N.L. Henderson, J.C. Bauer, D.W. Goodman, J.D. Batteas, R.E. Schaak, Synthesis of CuPt nanorod catalysts with tunable lengths, *J. Am. Chem. Soc.* 131 (2009) 5720–5721.

[38] Y.X. Zhang, M. Meng, F.F. Dai, T. Ding, R. You, States and function of potassium carbonate species in the polytitanate nanobelt supported catalysts used for efficient  $\text{NO}_x$  storage and reduction, *J. Phys. Chem. C* 117 (2013) 23691–23700.

[39] J.M. Moggia, V.G. Milt, M.A. Ulla, L.M. Cornaglia, Surface characterization of  $\text{Co}/\text{K}/\text{La}_2\text{O}_3$  catalysts used for the catalytic combustion of diesel soot, *Surf. Interface Anal.* 35 (2003) 216–225.

[40] M.M. Natile, A. Gisenti, New  $\text{NiO}/\text{Co}_3\text{O}_4$  and  $\text{Fe}_2\text{O}_3/\text{Co}_3\text{O}_4$  nanocomposite catalysts: synthesis and characterization, *Chem. Mater.* 15 (2003) 2502–2510.

[41] Y.E. Roginskaya, O.V. Morozova, E.N. Lubnin, Y.E. Ulitina, G.V. Lopukhova, S. Trasatti, Characterization of bulk and surface composition of  $\text{Co}_x\text{Ni}_{1-x}\text{O}_y$  mixed oxides for electrocatalysis, *Langmuir* 13 (1997) 4621–4627.

[42] Z.Q. Li, M. Meng, Y.Q. Zha, F.F. Dai, T.D. Hu, Y.N. Xie, J. Zhang, Highly efficient multifunctional dually-substituted perovskite catalysts  $\text{La}_{1-x}\text{K}_x\text{Co}_{1-y}\text{Cu}_y\text{O}_{3-\delta}$  used for soot combustion,  $\text{NO}_x$  storage and simultaneous  $\text{NO}_x$ -soot removal, *Appl. Catal. B* 121–122 (2012) 65–74.

[43] R.Q. Tan, Y.F. Zhu, Poisoning mechanism of perovskite  $\text{LaCoO}_3$  catalyst by organophosphorous gas, *Appl. Catal. B* 58 (2005) 61–68.

[44] A. Setiabudi, M. Makkee, J.A. Moulijn, An optimal  $\text{NO}_x$  assisted abatement of diesel soot in an advanced catalytic filter design, *Appl. Catal. B* 42 (2003) 35–45.

[45] J. Oi-Uchisawa, A. Obuchi, R. Enomoto, J.Y. Xu, T. Nanba, S. Liu, S. Kushiyama, Oxidation of carbon black over various  $\text{Pt}/\text{MO}_x/\text{SiC}$  catalysts, *Appl. Catal. B* 32 (2001) 257–268.

[46] S.T. Liu, A. Obuchi, J. Uchisawa, T. Nanba, S. Kushiyama, An exploratory study of diesel soot oxidation with  $\text{NO}_2$  and  $\text{O}_2$  on supported metal oxide catalysts, *Appl. Catal. B* 37 (2002) 309–319.

[47] C.A. Neyertz, E.D. Banús, E.E. Miró, C.A. Querini, Potassium-promoted  $\text{Ce}_{0.65}\text{Zr}_{0.35}\text{O}_2$  monolithic catalysts for diesel soot combustion, *Chem. Eng. J.* 248 (2014) 394–405.

[48] X.G. Li, Y.H. Dong, H. Xian, W.Y. Hernández, M. Meng, H.H. Zou, A.J. Ma, T.Y. Zhang, Z. Jiang, N. Tsubaki, P. Vernoux, De- $\text{NO}_x$  in alternative lean/rich atmospheres on  $\text{La}_{1-x}\text{Sr}_x\text{CoO}_3$  perovskites, *Energy Environ. Sci.* 4 (2011) 3351–3354.

[49] R. You, Y.X. Zhang, D.S. Liu, M. Meng, L.R. Zheng, J. Zhang, T.D. Hu,  $\text{YCeZrO}$  ternary oxide solid solution supported nonplatinic lean-burn  $\text{NO}_x$  trap catalysts using  $\text{LaCoO}_3$  perovskite as active phase, *J. Phys. Chem. C* 118 (2014) 25403–25420.

- [50] J.M. Christensen, J.D. Grunwaldt, A.D. Jensen, Effect of  $\text{NO}_2$  and water on the catalytic oxidation of soot, *Appl. Catal. B* 205 (2017) 182–188.
- [51] L. Cheng, Y. Men, J.G. Wang, H. Wang, W. An, Y.Q. Wang, Z.C. Duan, J. Liu, Crystal facet-dependent reactivity of  $\alpha\text{-Mn}_2\text{O}_3$  microcrystalline catalyst for soot combustion, *Appl. Catal. B* 204 (2017) 374–384.
- [52] N.D. Wasalathantri, T.M. SantaMaria, D.A. Kriz, S.L. Dissanayake, C.H. Kuo, S. Biswas, S.L. Suib, Mesoporous manganese oxides for  $\text{NO}_2$  assisted catalytic soot oxidation, *Appl. Catal. B* 201 (2017) 543–551.
- [53] R. Matarrese, S. Morandi, L. Castoldi, P. Villa, L. Lietti, Removal of  $\text{NO}_x$  and soot over  $\text{Ce/Zr/K/Me}$  ( $\text{Me} = \text{Fe, Pt Ru, Au}$ ) oxide catalysts, *Appl. Catal. B* 201 (2017) 318–330.
- [54] S.G. Chen, R.T. Yang, Unified mechanism of alkali and alkaline earth catalyzed gasification reactions of carbon by  $\text{CO}_2$  and  $\text{H}_2\text{O}$ , *Energy Fuels* 11 (1997) 421–427.
- [55] S. Matzner, H.P. Boehm, Influence of nitrogen doping on the adsorption and reduction of nitric oxide by activated carbons, *Carbon* 36 (1998) 1697–1709.
- [56] X. Wang, Y.X. Zhang, Q. Li, Z.P. Wang, Z. Zhang, Identification of active oxygen species for soot combustion on  $\text{LaMnO}_3$  perovskite, *Catal. Sci. Technol.* 2 (2012) 1822–1824.
- [57] Q. Li, X. Wang, Y. Xin, Z.L. Zhang, Y.X. Zhang, C. Hao, M. Meng, L.R. Zheng, L. Zheng, A unified intermediate and mechanism for soot combustion on potassium-supported oxides, *Sci. Rep.* 4 (2014) 4725–4731.